

# THE METAL–INSULATOR TRANSITION IN ONE DIMENSION

H.J. SCHULZ

Laboratoire de Physique des Solides

Université Paris–Sud, 91405 Orsay, France

**Abstract:** The low–energy excited states of a system of interacting one–dimensional fermions in a conducting state are collective charge and spin density oscillations. The unusual physical properties of such a system (called “Luttinger liquid”) are characterized by the velocities  $u_\rho$  and  $u_\sigma$  of the charge and spin excitations, as well as by a parameter  $K_\rho$  that determines the power law behavior of correlation functions. Umklapp scattering occurring at half–filling or other commensurate bandfilling can lead to a transition into an insulating state, characterized in particular by a gap in the charge excitations (the Mott–Hubbard gap). The properties in the vicinity of the transition are shown to depend on both the way the transition is approached (constant bandfilling and varying interaction, or constant interaction and varying bandfilling) and on the “order” of the commensurability. In particular, even and odd fractional fillings show quite different behavior. This behavior is illustrated in detail using lattice models like the Hubbard model and its extensions.

## 1 Introduction

A theoretical understanding of interacting fermion systems in one dimension is important for a number of reasons. On the one hand, in the physics of quasi-one-dimensional organic conductors [1] or of conducting polymers [2] interaction effects play a major role. On the other hand, one–dimensional models can be easier to understand than their higher-dimensional versions, or even exactly solvable, as is the case with the prototypical model of correlated fermions, the Hubbard model [3]. They therefore can provide valuable information on the role of correlation effects in higher dimension, e.g. on the physics of correlated fermions in two dimensions which is thought to be at the origin of the many interesting properties of high-temperature superconductors [4, 5].

Theoretical work on interacting fermions in one dimension has progressed along a number of different lines. One approach has been the perturbative investigation of the weak coupling limit. Even this is in fact not entirely straightforward, mainly because of the infrared divergences encountered in this type of calculation which re-

quire a renormalization group treatment. A complete review of this approach has been given by Sólyom [6]. An alternative and more general approach is provided by the so-called “bosonization” method, which is based on the equivalence between interacting fermions and noninteracting bosons (representing density fluctuations) and on the expression of fermionic operators in terms of these bosons. Combined with the renormalization group approach, the bosonization method provides a rather straightforward description of the peculiar properties of one-dimensional interacting fermion systems (“Luttinger liquid”), and one finds that the low-energy physical properties are determined by only three parameters: the velocities of collective charge- and spin-density oscillations ( $u_{\rho,\sigma}$ ), and a coefficient  $K_\rho$  that determines the long-distance decay of correlation functions. These coefficients play a role similar to the Landau parameters of (three-dimensional) Fermi liquid theory. A number of physical properties depending on these parameters are discussed below, but let us mention here that in particular the coefficient  $K_\rho$  is important in a much wider variety of phenomena: the temperature dependence of the NMR relaxation rate [7] or of X-ray scattering intensities [8], the energy dependence of photoemission spectra [9], the effect of impurities [10], or possible low-temperature ordered states in systems of coupled chains [11] all depend on it. A brief discussion of bosonization will be given in chapter 2, but for more detailed and rigorous derivations and results, the reader is referred to more specialized articles [12, 13].

As presented in sec. 2, the theory applies to translational invariant systems, and therefore one always has a conducting state. On the other hand, if one considers lattice systems, umklapp scattering breaks translational invariance. In sec. 3, I will show how this type of scattering can be incorporated into the bosonization formalism. One then finds insulating phases of the Mott-Hubbard type, with properties depending in an interesting way on the order of commensurability. There are two types of metal-insulator transitions: either at constant particle density, as a function of interaction strength, or at constant interaction, as a function of particle density. The “critical behavior” of the two types of transitions is quite different.

A rather different approach (at least until recently) is based on the famous “Bethe ansatz” [14] which in particular has made possible an exact solution of both continuum fermions interacting via  $\delta$ -function potentials [15, 16] and of the one-dimensional Hubbard model [3] (and of many other interesting models). In section 4 I will discuss the low-lying excitations of the one-dimensional Hubbard model as obtained from the exact solution. This will give a rather concrete illustration of the concept of “holons” and “spinons”. Moreover, one observes interesting changes as the metal-insulator transition is approached.

The exact Bethe ansatz eigenfunctions are so complicated that the direct calculation of correlation functions and many other physical properties of the one-dimensional Hubbard model is difficult even for very small systems [17] and impossible in the thermodynamic limit. In section 4.3 I present a method [18] that allows in particular a determination of the coefficient  $K_\rho$  for arbitrary correlation strength.

One then obtains a rather detailed *and exact* description of the low-energy (and low temperature) properties and also of the metal-insulator transition occurring when the average particle number per site,  $n$ , approaches unity. The method generalizes rather straightforwardly to other models, where however in general one has to rely on exact calculations for small systems and an extrapolation to the thermodynamic limit.

## 2 Luttinger liquids

### 2.1 The spinless case

#### 2.1.1 The model and its solution

Let us consider the standard case of an interacting fermion model with the Hamiltonian consisting of two parts: the kinetic energy and the interaction. Omitting spin for the moment, the kinetic energy term is of the form

$$H_0 = \sum_k \varepsilon_k c_k^\dagger c_k \quad , \quad (2.1)$$

where  $c_k$  and  $c_k^\dagger$  are the standard annihilation and creation operators for a fermion with momentum  $k$ , and  $\varepsilon_k$  is the single-particle bandstructure. In a simple tight-binding model one would have  $\varepsilon_k = -2t \cos k$  (the lattice constant is set to unity), but the precise form of  $\varepsilon_k$  is unimportant here. The Fermi surface consists just of the two points  $\pm k_F$ .

For weak interactions between the particles, only states in the immediate vicinity of the Fermi points are important. For these states, one then can linearize the electronic dispersion relation around the Fermi points, and the kinetic energy term takes the form

$$H_0 = v_F \sum_k \{ (k - k_F) a_k^\dagger a_k + (-k - k_F) b_k^\dagger b_k \} \quad . \quad (2.2)$$

Here the  $a$  ( $b$ ) operators refer to states in the vicinity of  $+k_F$  ( $-k_F$ ), i.e. the  $a$ -particles move to the right, the  $b$ -particles move to the left. The  $k$ -summation is limited to an interval  $[-k_0, k_0]$  around  $k_F$  (typically,  $k_0 \approx \pi/2$ , but the precise value isn't important here). The Fermi velocity is given by

$$v_F = \left. \frac{\partial \varepsilon_k}{\partial k} \right|_{k_F} \quad , \quad (2.3)$$

and the density of states is  $N(E_F) = 1/(\pi v_F)$ . In the *Luttinger model*, one generalizes this kinetic energy by letting the cutoff  $k_0$  tend to infinity. There then are two branches of particles, “right movers” and “left movers”, both with unconstrained momentum and energy. At least for weak interaction, this addition of extra states far from the Fermi energy is not expected to change the physics much. However,

this modification makes the model exactly solvable even in the presence of nontrivial interactions. Moreover, and most importantly, many of the features of this model carry over even to strongly interacting fermions on a lattice.

We now introduce interactions between the fermions. As long as only forward scattering of the type  $(k_F; -k_F) \rightarrow (k_F; -k_F)$  or  $(k_F; k_F) \rightarrow (k_F; k_F)$  is introduced, the model remains exactly solvable. Introducing the Fourier components of the particle density operator for right and left movers by

$$\rho_+(q) = \sum_k a_{k+q}^\dagger a_k \quad , \quad \rho_-(q) = \sum_k b_{k+q}^\dagger b_k \quad , \quad (2.4)$$

the interaction Hamiltonian describing these processes takes the form

$$H_{int} = \frac{1}{2L} \sum_q \{2g_2(q)\rho_+(q)\rho_-(-q) + g_4(q)[\rho_+(q)\rho_+(-q) + \rho_-(-q)\rho_-(q)]\} . \quad (2.5)$$

Here,  $g_2(q)$  and  $g_4(q)$  are the Fourier transforms of a real space interaction potential, and in a realistic case one would of course have  $g_2(q) = g_4(q)$ , but it is useful to allow for differences between  $g_2$  and  $g_4$ . For Coulomb interactions one expects  $g_2, g_4 > 0$ . In principle, the long-range part of the Coulomb repulsion leads to a singular  $q$ -dependence. Such singularities in the  $g_i$  can be handled rather straightforwardly and can lead to interesting physical effects [19], but here I shall limit myself mainly to nonsingular  $g_2, g_4$ . Electron-phonon interactions can lead to effectively attractive interactions between electrons, and therefore in the following I will not make any restrictive assumptions about the sign of the constants. One should however notice that a proper treatment of the phonon dynamics and of the resulting retardation effects requires more care [20].

The model defined by eqs. (2.2) and (2.5) can be solved exactly. The solution is based on the following facts:

1. the density fluctuation operators  $\rho_\pm$  obey Bose type commutation relations:

$$[\rho_+(-q), \rho_+(q')] = [\rho_-(-q), \rho_-(-q')] = \delta_{qq'} \frac{qL}{2\pi} \quad , \quad [\rho_+(q), \rho_-(q')] = 0 \quad . \quad (2.6)$$

Moreover, for  $q > 0$  both  $\rho_+(-q)$  and  $\rho_-(q)$  annihilate the noninteracting groundstate. These properties are closely related to the existence of an infinity of states at negative energies and would not have been true in a lattice system like the one described by (2.1).

2. The kinetic part of the Hamiltonian can be re-written as a term bilinear in boson operators, i.e. quartic in fermion operators:

$$H_0 = \frac{2\pi v_F}{L} \sum_{q>0} [\rho_+(q)\rho_+(-q) + \rho_-(-q)\rho_-(q)] \quad . \quad (2.7)$$

This equivalence may be made plausible noting that  $\rho_+(q)$  creates particle–hole pairs that all have total momentum  $q$ . Their energy is  $\varepsilon_{k+q} - \varepsilon_k$ , which, because of the linearity of the spectrum equals  $v_F q$ , *independently of  $k$* . Thus, states created by  $\rho_+(q)$  are linear combinations of individual electron–hole excitations all with the same energy, and therefore are also eigenstates of (2.2).

3. The states created by repeated application of  $\rho_{\pm}$  on the ground state form a complete set of basis states [13, 21].

Putting together (2.7) and (2.5), the complete interacting Hamiltonian then becomes a bilinear form in boson operators, that is easily diagonalized by a Bogolyubov transformation. A first consequence is the expression for the excitation spectrum

$$\omega(q) = |q|[(v_F + g_4(q)/(2\pi))^2 - (g_2(q)/(2\pi))^2]^{1/2} . \quad (2.8)$$

The diagonal boson operators are linear combinations of the original  $\rho$  operators, and consequently, these elementary excitations are collective density oscillations, their energy being determined both by the kinetic energy term and the interactions.

We note here that in order for the Bogolyubov transformation to be a well–defined unitary transformation,  $g_2(q)$  has to decrease at large  $q$  at least as  $|q|^{-1/2}$ . on the other hand, the large– $q$  behavior of  $g_2$  is unimportant for the low–energy properties of the model. We therefore in the following will almost always use a  $q$ –independent  $g_2$  and  $g_4$ . An approximate and frequently used way to cure the divergences arising due to this procedure is to keep the parameter  $\alpha$  in subsequent formulae as a finite short–distance cutoff, of the order of a lattice spacing. One can then also include the “backward scattering”  $(k_F; -k_F) \rightarrow (-k_F; k_F)$ , because for spinless electron this is just the exchange analogue of forward scattering and does not constitute a new type of interaction.

Up to this point, this construction does not allow for a direct calculation of correlation functions like the one–particle Green’s function or more generally any function involving individual creation or destruction operators. This type of correlation function becomes tractable by representing single particle operators in terms of the boson operators; To this end, we introduce the field operators

$$\phi(x) = -\frac{i\pi}{L} \sum_{p \neq 0} \frac{1}{p} e^{-\alpha|p|/2 - ipx} [\rho_+(p) + \rho_-(p)] - N \frac{\pi x}{L} , \quad (2.9)$$

$$\Pi(x) = \frac{1}{L} \sum_{p \neq 0} e^{-\alpha|p|/2 - ipx} [\rho_+(p) - \rho_-(p)] + J/L . \quad (2.10)$$

Here  $N$  and  $J$  are the number of particles added to the ground state and the difference between the number of right and left–moving particles, respectively, and  $\alpha$  is a cutoff parameter which (at least in principle, see the discussion above) has to be set to zero in the end of any calculation.  $\phi$  and  $\Pi$  obey canonical boson commutation, relations:

$$[\phi(x), \Pi(y)] = i\delta(x - y) , \quad (2.11)$$

and  $\phi$  is related to the local particle density via  $\partial\phi/\partial x = -\pi\rho(x)$ . The expression for the single fermion operators then is

$$\psi_{\pm}(x) = \lim_{\alpha \rightarrow 0} \frac{1}{\sqrt{2\pi\alpha}} \exp[\pm ik_F x \mp i\phi(x) - i\theta(x)] \quad , \quad (2.12)$$

where  $\theta(x) = \pi \int^x \Pi(x') dx'$ , and the upper and lower sign refer to right- and left-moving electrons, respectively. A detailed derivation of this important relation as an operator identity is given in the literature [13, 21]. However, a simple plausibility argument can be given: creating a particle at site  $x$  means introducing a kink of height  $\pi$  in  $\phi$ , i.e. at points on the left of  $x$   $\phi$  has to be shifted by  $\pi$ . Displacement operators are exponentials of momentum operators, and therefore a first guess would be  $\psi^{\dagger}(x) \approx \exp(i\pi \int_{-\infty}^x \Pi(x') dx')$ . However, this operator commutes with itself, instead of satisfying canonical anticommutation relations. Anticommutation is achieved by multiplying with an operator, acting at site  $x$ , that changes sign each time a particle passes through  $x$ . Such an operator is  $\exp(\pm i\phi(x))$ . The product of these two factors then produces (2.29).

The full Hamiltonian can also be simply expressed in terms of  $\phi$  and  $\Pi$ . Neglecting the momentum dependence of the  $g_i$ , one easily finds

$$H = H_0 + H_{int} = \int dx \left[ \frac{\pi u K}{2} \Pi(x)^2 + \frac{u}{2\pi K} (\partial_x \phi)^2 \right] \quad . \quad (2.13)$$

This is obviously just the Hamiltonian of an elastic string, with the eigenmodes corresponding to the collective density fluctuations of the fermion liquid. It is important to notice that these collective modes are the only (low-energy) excited states, and that in particular *there are no well-defined single particle excitations*. The parameters in (2.13) are given by

$$u = [(v_F + g_4/(2\pi))^2 - g_2^2/(2\pi)^2]^{1/2} \quad , \quad K = \left[ \frac{2\pi v_F + g_4 - g_2}{2\pi v_F + g_4 + g_2} \right]^{1/2} \quad . \quad (2.14)$$

The energies of the eigenstates are  $\omega(q) = u|q|$ , in agreement with eq. (2.8).

### 2.1.2 Physical properties

The simple form of the Hamiltonian (2.13) makes the calculation of physical properties rather straightforward. First note that acoustic phonons in one dimension have a linear specific heat. Consequently, the low-temperature specific heat of interacting fermions is  $C(T) = \gamma T$ , with

$$\gamma/\gamma_0 = v_F/u \quad . \quad (2.15)$$

Here  $\gamma_0$  is the specific heat coefficient of noninteracting electrons of Fermi velocity  $v_F$ . Also, the coefficient  $u/K$  fixes the energy needed to change the particle density, and consequently the renormalization of the compressibility  $\kappa$  is given by

$$\kappa/\kappa_0 = v_F K/u \quad , \quad (2.16)$$

where  $\kappa_0$  is the compressibility of the noninteracting case.

The quantity  $\Pi$  is proportional to the current density. Obviously, the Hamiltonian commutes with the total current, and therefore the frequency dependent conductivity is a delta function at  $\omega = 0$ . Using the Kubo formula, one straightforwardly finds

$$\sigma(\omega) = Ku\delta(\omega) \quad , \quad (2.17)$$

i.e. the product  $Ku$  determines the weight of the dc peak in the conductivity.

The above properties are those of an ordinary Fermi liquid, the coefficients  $u$ , and  $K$  determining renormalizations with respect to noninteracting quantities. We will now consider quantities which show that a one-dimensional interacting fermion system is *not a Fermi liquid*. Consider the single-particle Green's function which can be calculated using the representation (2.12) of fermion operators:

$$\begin{aligned} G^R(x, t) &= -i\theta(t)\langle[\psi_+(x, t), \psi_+^\dagger(0, 0)]_+\rangle \\ &= -\frac{\theta(t)}{\pi}e^{ik_F x}\text{Re}\left\{\frac{1}{ut-x}\left[\frac{\alpha^2}{(\alpha+iut)^2+x^2}\right]^{\delta/2}\right\} . \end{aligned} \quad (2.18)$$

One then finds for the momentum distribution function in the vicinity of  $k_F$ :

$$n_k \approx n_{k_F} - \text{const.}\text{sign}(k - k_F)|k - k_F|^\delta \quad , \quad (2.19)$$

and for the single-particle density of states:  $N(\omega) \approx |\omega|^\delta$ , with  $\delta = (K + 1/K - 2)/4$ , and  $\beta$  is a model-dependent constant. Note that for any  $K \neq 1$ , i.e. *for any nonvanishing interaction*, the momentum distribution function and the density of states have power-law singularities at the Fermi level, with a vanishing single particle density of states at  $E_F$ . This behavior is obviously quite different from a standard Fermi liquid which would have a finite density of states and a step-like singularity in  $n_k$ . The absence of a step at  $k_F$  in the momentum distribution function implies the *absence of a quasiparticle pole* in the one-particle Green's function. Instead one finds in the spectral function  $A(k, \omega)$  a continuum above a threshold  $u(k - k_F)$ , with a singularity close to the threshold:  $A(k, \omega) \propto (\omega - u(k - k_F))^{\delta-1}$ , and there is also some (non-divergent) spectral weight at negative energies [22, 23, 24].

The coefficient  $K$  also determines the long-distance decay of all other correlation functions of the system: in the present context the most interesting correlations are those involving charge density or pairing fluctuations. Using the representation (2.12) the corresponding operators can be written as

$$O_{CDW}(x) = \psi_-^\dagger(x)\psi_+(x) = \lim_{\alpha \rightarrow 0} \frac{e^{2ik_F x}}{\pi\alpha} e^{-2i\phi(x)} \quad , \quad (2.20)$$

$$O_{SC}(x) = \psi_-(x)\psi_+(x) = \lim_{\alpha \rightarrow 0} \frac{1}{\pi\alpha} e^{-2i\theta(x)} \quad . \quad (2.21)$$

Similar relations can also be found for other operators. The CDW and pairing correlation functions now are easily calculated as a function of  $x$ ,  $t$ , and temperature [12].

I here only give the leading asymptotic behavior at zero temperature:

$$\begin{aligned}\langle O_{CDW}^\dagger(x,t)O_{CDW}(0) \rangle &= C_1(x^2 - u^2t^2)^{-K} , \\ \langle O_{SC}^\dagger(x,t)O_{SC}(0) \rangle &= C_2(x^2 - u^2t^2)^{-1/K} ,\end{aligned}\quad (2.22)$$

with interaction–dependent constants  $C_{1,2}$ . The corresponding susceptibilities (i.e. the Fourier transforms of the above correlation functions) behave at low temperatures as

$$\chi_{CDW}(T) \approx T^{2K-2} , \chi_{SC}(T) \approx T^{2/K-2} , \quad (2.23)$$

i.e. for  $K < 1$  charge density fluctuations at  $2k_F$  are enhanced and diverge at low temperatures, whereas for  $K > 1$  pairing fluctuations dominate. The remarkable fact in all the above results is that there is only *one coefficient*,  $K$ , which determines all the asymptotic power laws.

To summarize the spinless case, we have found striking differences with the usual Fermi liquid picture: there are no quasiparticle poles in the single–particle Green’s function, but rather power law singularities, with interaction–dependent exponents. Similar power laws appear in all types of correlation functions. However, all exponents are related to one parameter  $K$ , which contains all the interaction dependence. This type of behavior has been called **Luttinger liquid** by Haldane [13].

## 2.2 Spin–1/2 fermions

In the case of spin–1/2 fermions, all the fermion operators acquire an additional spin index  $s$ . Following the same logic as above, the kinetic energy then takes the form

$$\begin{aligned}H_0 &= v_F \sum_{k,s} \{ (k - k_F) a_{k,s}^\dagger a_{k,s} + (-k - k_F) b_{k,s}^\dagger b_{k,s} \} \\ &= \frac{2\pi v_F}{L} \sum_{q>0,s} [\rho_{+,s}(q)\rho_{+,s}(-q) + \rho_{-,s}(-q)\rho_{-,s}(q)] ,\end{aligned}\quad (2.24)$$

where density operators for spin projections  $s = \uparrow, \downarrow$  have been introduced:

$$\rho_{+,s}(q) = \sum_k a_{k+q,s}^\dagger a_{k,s} , \quad \rho_{-,s}(q) = \sum_k b_{k+q,s}^\dagger b_{k,s} . \quad (2.25)$$

There are now two types of interaction. First, the “backward scattering”  $(k_F, s; -k_F, t) \rightarrow (-k_F, s; k_F, t)$  which for  $s \neq t$  cannot be re–written as an effective forward scattering (contrary to the spinless case). The corresponding Hamiltonian is

$$H_{int,1} = \frac{1}{L} \sum_{kpqst} g_1 a_{k,s}^\dagger b_{p,t}^\dagger a_{p+2k_F+q,t} b_{k-2k_F-q,s} . \quad (2.26)$$

And, of course, there is also the forward scattering, of a form similar to the spinless case

$$H_{int,2} = \frac{1}{2L} \sum_{qst} \{ 2g_2(q)\rho_{+,s}(q)\rho_{-,t}(-q) \quad (2.27)$$

$$+ g_4(q)[\rho_{+,s}(q)\rho_{+,t}(-q) + \rho_{-,s}(-q)\rho_{-,t}(q)] \} . \quad (2.28)$$



To go to the bosonic description, one introduces  $\phi$  and  $\Pi$  fields for the two spin projections separately, and then transforms to charge and spin bosons via  $\phi_{\rho,\sigma} = (\phi_{\uparrow} \pm \phi_{\downarrow})/\sqrt{2}$ ,  $\Pi_{\rho,\sigma} = (\Pi_{\uparrow} \pm \Pi_{\downarrow})/\sqrt{2}$ . The operators  $\phi_{\nu}$  and  $\Pi_{\nu}$  obey Bose-like commutation relations:

$$[\phi_{\nu}(x), \Pi_{\mu}(y)] = i\delta_{\nu\mu}\delta(x-y) \quad ,$$

and single fermion operators can be written in a form analogous to (2.12):

$$\psi_{\pm,s}(x) = \lim_{\alpha \rightarrow 0} \frac{1}{\sqrt{2\pi\alpha}} \exp \left[ \pm ik_F x - i(\pm(\phi_{\rho} + s\phi_{\sigma}) - (\theta_{\rho} + s\theta_{\sigma}))/\sqrt{2} \right] \quad , \quad (2.29)$$

where  $\theta_{\nu}(x) = \pi \int^x \Pi_{\nu}(x') dx'$ .

The full Hamiltonian  $H = H_0 + H_{int,1} + H_{int,2}$  then takes the form

$$H = H_{\rho} + H_{\sigma} + \frac{2g_1}{(2\pi\alpha)^2} \int dx \cos(\sqrt{8}\phi_{\sigma}) \quad . \quad (2.30)$$

Here  $\alpha$  is a short-distance cutoff, and for  $\nu = \rho, \sigma$

$$H_{\nu} = \int dx \left[ \frac{\pi u_{\nu} K_{\nu}}{2} \Pi_{\nu}^2 + \frac{u_{\nu}}{2\pi K_{\nu}} (\partial_x \phi_{\nu})^2 \right] \quad , \quad (2.31)$$

with

$$u_{\nu} = [(v_F + g_{4,\nu}/\pi)^2 - g_{\nu}^2/(2\pi)^2]^{1/2} \quad , \quad K_{\nu} = \left[ \frac{2\pi v_F + 2g_{4,\nu} + g_{\nu}}{2\pi v_F + 2g_{4,\nu} - g_{\nu}} \right]^{1/2} \quad , \quad (2.32)$$

and  $g_{\rho} = g_1 - 2g_2$ ,  $g_{\sigma} = g_1$ ,  $g_{4,\rho} = g_4$ ,  $g_{4,\sigma} = 0$ . For a noninteracting system one thus has  $u_{\nu} = v_F$  (charge and spin velocities equal!) and  $K_{\nu} = 1$ . For  $g_1 = 0$ , (2.30) describes independent long-wavelength oscillations of the charge and spin density, with linear dispersion relation  $\omega_{\nu}(k) = u_{\nu}|k|$ , and the system is conducting. As in the spinless case, there are no single-particle or single particle-hole pair excited states. This model (no backscattering), usually called the Tomonaga-Luttinger model, is the one to which the bosonization method was originally applied [25, 26, 27].

For  $g_1 \neq 0$  the cosine term has to be treated perturbatively. A straightforward calculation gives the renormalization group equation

$$\frac{d}{dl} g_1(l) = \frac{1}{\pi v_F} g_1(l)^2 \quad , \quad \frac{d}{dl} g_2(l) = \frac{1}{2\pi v_F} g_1(l)^2 \quad , \quad (2.33)$$

where the renormalized cutoff  $E_c$  is related to the bare cutoff  $E_0$  via  $E_c = E_0 \exp(l)$ . Thus, for repulsive interactions ( $g_1 > 0$ ),  $g_1$  is renormalized to zero in the long-wavelength limit, and at the fixed point one has  $K_{\sigma}^* = 1$ . The three remaining parameters in (2.30) then completely determine the long-distance and low-energy properties of the system.

It should be emphasized that (2.30) has been derived here for fermions with linear energy-momentum relation. For more general (e.g. lattice) models, there

are additional operators arising from band curvature and the absence of high-energy single-particle states. One can however show that all these effects are, at least for not very strong interaction, irrelevant in the renormalization group sense, i.e. they do not affect the low-energy physics. Thus, (2.30) is still the correct effective Hamiltonian for low-energy excitations.

The Hamiltonian (2.30) also provides an explanation for the physics of the case of negative  $g_1$ , where the renormalization group scales to strong coupling (eq.(2.33)). In fact, if  $|g_1|$  is large in (2.30), it is quite clear that the elementary excitations of  $\phi_\sigma$  will be small oscillations around one of the minima of the cos term, or possibly soliton-like objects where  $\phi_\sigma$  goes from one of the minima to the other. Both types of excitations have a gap, i.e. for  $g_1 < 0$  one has a *gap in the spin excitation spectrum*, whereas the charge excitations remain massless. This can actually be investigated in more detail in an exactly solvable case [28].

### 2.2.1 Spin-charge separation

One of the more spectacular consequences of the Hamiltonian (2.30) is the complete separation of the dynamics of the spin and charge degrees of freedom. For example, in general one has  $u_\sigma \neq u_\rho$ , i.e. the charge and spin oscillations propagate with different velocities. Only in a noninteracting system or if some accidental degeneracy occurs does one have  $u_\sigma = u_\rho = v_F$ . To make the meaning of this fact more transparent, let us create an extra particle in the ground state, at  $t = 0$  and spatial coordinate  $x_0$ . The charge and spin densities then are easily found, using  $\rho(x) = -(\sqrt{2}/\pi)\partial\phi_\rho/\partial x$  (note that  $\rho(x)$  is the deviation of the density from its average value) and  $\sigma_z(x) = -(\sqrt{2}/\pi)\partial\phi_\sigma/\partial x$  :

$$\begin{aligned} \langle 0|\psi_+(x_0)\rho(x)\psi_+^\dagger(x_0)|0\rangle &= \delta(x - x_0) , \\ \langle 0|\psi_+(x_0)\sigma_z(x)\psi_+^\dagger(x_0)|0\rangle &= \delta(x - x_0) . \end{aligned} \tag{2.34}$$

Now, consider the time development of the charge and spin distributions. The time-dependence of the charge and spin density operators is easily obtained from (2.30) (using the fixed point value  $g_1 = 0$ ), and one obtains

$$\begin{aligned} \langle 0|\psi_+(x_0)\rho(x,t)\psi_+^\dagger(x_0)|0\rangle &= \delta(x - x_0 - u_\rho t) , \\ \langle 0|\psi_+(x_0)\sigma_z(x,t)\psi_+^\dagger(x_0)|0\rangle &= \delta(x - x_0 - u_\sigma t) . \end{aligned} \tag{2.35}$$

Because in general  $u_\sigma \neq u_\rho$ , after some time charge and spin will be localized at completely different points in space, i.e. *charge and spin have separated completely*. A interpretation of this surprising phenomenon in terms of the Hubbard model will be given in sec.(4).

Here a linear energy-momentum relation has been assumed for the electrons, and consequently the shape of the charge and spin distributions is time-independent. If the energy-momentum relation has some curvature (as is necessarily the case in lattice systems) the distributions will widen with time. However this widening is

proportional to  $\sqrt{t}$ , and therefore much smaller than the distance between charge and spin. Thus, the qualitative picture of spin-charge separation is unchanged.

### 2.2.2 Physical properties

The simple form of the Hamiltonian (2.30) at the fixed point  $g_1^* = 0$  makes the calculation of physical properties rather straightforward. The specific heat now is determined both by the charge and spin modes, and consequently the specific heat coefficient  $\gamma$  is given by

$$\gamma/\gamma_0 = \frac{1}{2}(v_F/u_\rho + v_F/u_\sigma) . \quad (2.36)$$

Here  $\gamma_0$  is the specific heat coefficient of noninteracting electrons of Fermi velocity  $v_F$ .

The spin susceptibility and the compressibility are equally easy to obtain. Note that in (2.30) the coefficient  $u_\sigma/K_\sigma$  determines the energy necessary to create a nonzero spin polarization, and, as in the spinless case,  $u_\rho/K_\rho$  fixes the energy needed to change the particle density. Given the fixed point value  $K_\sigma^* = 1$ , one finds

$$\chi/\chi_0 = v_F/u_\sigma \quad , \quad \kappa/\kappa_0 = v_F K_\rho/u_\rho \quad , \quad (2.37)$$

where  $\chi_0$  and  $\kappa_0$  are the susceptibility and compressibility of the noninteracting case. From eqs.(2.36) and (2.37) the Wilson ratio is

$$R_W = \frac{\chi}{\gamma} \frac{\gamma_0}{\chi_0} = \frac{2u_\rho}{u_\rho + u_\sigma} . \quad (2.38)$$

The quantity  $\Pi_\rho(x)$  is proportional to the current density. As before, the Hamiltonian commutes with the total current, one thus has

$$\sigma(\omega) = 2K_\rho u_\rho \delta(\omega) + \sigma_{reg}(\omega) \quad , \quad (2.39)$$

i.e. the product  $K_\rho u_\rho$  determines the weight of the dc peak in the conductivity. The regular part of the conductivity in general varies as  $\omega^3$  at low frequencies [29].

The above properties, linear specific heat, finite spin susceptibility, and dc conductivity are those of an ordinary Fermi liquid, the coefficients  $u_\rho$ ,  $u_\sigma$ , and  $K_\rho$  determining renormalizations with respect to noninteracting quantities. However, the present system is *not a Fermi liquid*. This is in fact already obvious from the preceding discussion on charge–spin separation, and can be made more precise considering the single–particle Green’s function. Using the representation (2.29) of fermion operators one finds (at the fixed point  $g_1 = 0$ )

$$\begin{aligned} G^R(x, t) &= -i\theta(t) \langle [\psi_{+,s}(x, t), \psi_{+,s}^\dagger(0, 0)]_+ \rangle \\ &= -\frac{\theta(t)}{\pi} e^{ik_F x} \text{Re} \left\{ \frac{1}{\sqrt{(u_\rho t - x)(u_\sigma t - x)}} \left[ \frac{\alpha^2}{(\alpha + iu_\rho t)^2 + x^2} \right]^{\delta/2} \right\} \end{aligned} \quad (2.40)$$

Note that this expression factorizes into a spin and a charge contribution which propagate with different velocities. Fourier transforming (2.40) gives the momentum distribution function in the vicinity of  $k_F$ :

$$n_k \approx n_{k_F} - \text{const. sign}(k - k_F) |k - k_F|^\delta \quad , \quad (2.41)$$

and for the single-particle density of states (i.e. the momentum-integrated spectral density) one finds:

$$N(\omega) \approx |\omega|^\delta \quad . \quad (2.42)$$

In both cases  $\delta = (K_\rho + 1/K_\rho - 2)/4$ . Note that for any  $K_\rho \neq 1$ , i.e. *for any nonvanishing interaction*, the momentum distribution function and the density of states have power-law singularities at the Fermi level, with a vanishing single particle density of states at  $E_F$ . This behavior is obviously quite different from a standard Fermi liquid which would have a finite density of states and a step-like singularity in  $n_k$ . The absence of a step at  $k_F$  in the momentum distribution function implies the *absence of a quasiparticle pole* in the one-particle Green's function. In fact, a direct calculation of the spectral function  $A(k, \omega)$  from (2.40) [23, 24] shows that the usual quasiparticle pole is replaced by a continuum, with a lower threshold at  $\min(u_\nu)(k - k_F)$  and branch cut singularities at  $\omega = u_\rho p$  and  $\omega = u_\sigma p$ :

$$A(k, \omega) \approx (\omega - u_\sigma(k - k_F))^{\delta-1/2} \quad , \quad |\omega - u_\rho(k - k_F)|^{(\delta-1)/2} \quad (u_\rho > u_\sigma) \quad , \quad (2.43)$$

$$A(k, \omega) \approx (\omega - u_\rho(k - k_F))^{\delta-1/2} \quad , \quad |\omega - u_\sigma(k - k_F)|^{\delta-1/2} \quad (u_\rho < u_\sigma) \quad . \quad (2.44)$$

The coefficient  $K_\rho$  also determines the long-distance decay of all other correlation functions of the system: Using the representation (2.29) the charge and spin density operators at  $2k_F$  are

$$O_{CDW}(x) = \sum_s \psi_{-,s}^\dagger(x) \psi_{+,s}(x) = \lim_{\alpha \rightarrow 0} \frac{e^{2ik_F x}}{\pi\alpha} e^{-i\sqrt{2}\phi_\rho(x)} \cos[\sqrt{2}\phi_\sigma(x)] \quad , \quad (2.45)$$

$$O_{SDW_x}(x) = \sum_s \psi_{-,s}^\dagger(x) \psi_{+,-s}(x) = \lim_{\alpha \rightarrow 0} \frac{e^{2ik_F x}}{\pi\alpha} e^{-i\sqrt{2}\phi_\rho(x)} \cos[\sqrt{2}\theta_\sigma(x)] \quad . \quad (2.46)$$

Similar relations are also found for other operators. It is important to note here that all these operators decompose into a product of one factor depending on the charge variable only by another factor depending only on the spin field. Using the Hamiltonian (2.30) at the fixed point  $g_1^* = 0$  one finds for example for the charge and spin correlation functions\*

$$\begin{aligned} \langle n(x)n(0) \rangle &= K_\rho/(\pi x)^2 + A_1 \cos(2k_F x) x^{-1-K_\rho} \ln^{-3/2}(x) \\ &\quad + A_2 \cos(4k_F x) x^{-4K_\rho} + \dots \quad , \end{aligned} \quad (2.47)$$

$$\langle \mathbf{S}(x) \cdot \mathbf{S}(0) \rangle = 1/(\pi x)^2 + B_1 \cos(2k_F x) x^{-1-K_\rho} \ln^{1/2}(x) + \dots \quad , \quad (2.48)$$

---

\*The time- and temperature dependence is also easily obtained, see [12].

with model dependent constants  $A_i, B_i$ . The ellipses in (2.47) and (2.48) indicate higher harmonics of  $\cos(2k_F x)$  which are present but decay faster than the terms shown here. Similarly, correlation functions for singlet (SS) and triplet (TS) superconducting pairing are

$$\begin{aligned}\langle O_{SS}^\dagger(x)O_{SS}(0) \rangle &= Cx^{-1-1/K_\rho} \ln^{-3/2}(x) + \dots , \\ \langle O_{TS_\alpha}^\dagger(x)O_{TS_\alpha}(0) \rangle &= Dx^{-1-1/K_\rho} \ln^{1/2}(x) + \dots .\end{aligned}\tag{2.49}$$

The logarithmic corrections in these functions [30] have been studied in detail recently [31, 32, 33, 34]. The corresponding susceptibilities (i.e. the Fourier transforms of the above correlation functions) behave at low temperatures as

$$\chi_{CDW}(T) \approx T^{K_\rho-1} |\ln(T)|^{-3/2} , \chi_{SDW}(T) \approx T^{K_\rho-1} |\ln(T)|^{1/2} ,\tag{2.50}$$

$$\chi_{SS}(T) \approx T^{1/K_\rho-1} |\ln(T)|^{-3/2} , \chi_{TS}(T) \approx T^{1/K_\rho-1} |\ln(T)|^{1/2} ,\tag{2.51}$$

i.e. for  $K_\rho < 1$  (spin or charge) density fluctuations at  $2k_F$  are enhanced and diverge at low temperatures, whereas for  $K_\rho > 1$  pairing fluctuations dominate. These correlation functions with their power law variations actually determine experimentally accessible quantities: the  $2k_F$  and  $4k_F$  charge correlations lead to X-ray scattering intensities  $I_{2k_F} \approx T^{K_\rho}$ ,  $I_{4k_F} \approx T^{4K_\rho-1}$ , and similarly the NMR relaxation rate due to  $2k_F$  spin fluctuations varies as  $1/T_1 \approx T^{K_\rho}$ . The remarkable fact in all the above results is that there is only *one coefficient*,  $K_\rho$ , which determines all the asymptotic power laws.

Correlation functions in the spin-1/2 case (“spin-1/2 Luttinger liquid”) share one important property with spinless fermions: they have power-law behavior, with interaction-dependent powers determined by one coefficient,  $K_\rho$ . However, the phenomenon of spin-charge separation adds some additional features in this case and has spectacular consequences both for thermodynamical and spectral properties.

## 3 Umklapp scattering and metal-insulator transitions

### 3.1 Half-filling

In the model discussed in the preceding section, total momentum was always a conserved quantity, and consequently these models are metallic with an infinite dc conductivity. However, in a half-filled band one has  $k_F = \pi/2$ . Then umklapp scattering, transferring two particles from  $-k_F$  to  $k_F$ , involves momentum transfer  $4k_F = 2\pi$  which is a reciprocal lattice vector. These processes are thus allowed and lead to an extra term

$$H_{int,3} = \frac{1}{L} \sum_{k p q s} g_3 (a_{k,s}^\dagger a_{p,-s}^\dagger b_{p-2k_F+q,-s} b_{k-2k_F-q,s} + h.c.) .\tag{3.1}$$

in the Hamiltonian. Note that because of the Pauli principle, only scattering of two particles of opposite spin is allowed if, as usually is assumed,  $g_3$  is momentum-independent. In the boson representation, this term leads to an additional interaction for the charge degrees of freedom:

$$H_{int,3} = \frac{2g_3}{(2\pi\alpha)^2} \int dx \cos(\sqrt{8}\phi_\rho) . \quad (3.2)$$

Similarly to the  $g_1$  term, this term can be handled via a renormalization group calculation. The equations are

$$\frac{d}{dl}g_3(l) = \frac{1}{\pi v_F}(g_1(l) - 2g_2(l))g_3(l) , \quad \frac{d}{dl}(g_1(l) - 2g_2(l)) = \frac{1}{\pi v_F}g_3(l)^2 . \quad (3.3)$$

These in fact are the well-known Kosterlitz–Thouless equations. There are two regimes: (i) for  $|g_3| \leq g_1 - 2g_2$   $g_3$  scales to zero, and  $g_1 - 2g_2$  to the fixed point value  $(g_1 - 2g_2)^* = [(g_1 - 2g_2)^2 - g_3^2]^{1/2}$ . Consequently, the charge excitation spectrum remains massless, but there are corrections of order  $g_3^2$  to  $K_\rho$ : in eq (2.32) for  $K_\rho$  one replaces  $g_1 - 2g_2 \rightarrow (g_1 - 2g_2)^*$ , but  $u_\rho$  is unrenormalized at this order. Of course, in this case the system remains a metal. (ii) for  $|g_3| > g_1 - 2g_2$   $g_3$  scales towards strong coupling. From eq.(3.2) one then expects  $\phi_\rho$  to be essential fixed to one of the minima of the cosine potential. This gives rise to a gap in the charge excitation spectrum [35, 6]. The ground state then is insulating.

In a particular but illuminating case, the umklapp problem can be solved exactly [35]: after the unitary transformation  $\phi_\rho \rightarrow \phi_\rho/\sqrt{2}$ ,  $\Pi_\rho \rightarrow \sqrt{2}\Pi_\rho$ , the total Hamiltonian for the charge degrees of freedom becomes

$$H_\rho = \int dx \left[ \pi u_\rho K_\rho \Pi_\rho^2 + \frac{u_\rho}{4\pi K_\rho} (\partial_x \phi_\rho)^2 \right] + \frac{2g_3}{(2\pi\alpha)^2} \int dx \cos(2\phi_\rho) . \quad (3.4)$$

Using the transformations discussed in sec. 2, this problem can be transformed into a spinless fermion model. In particular, for  $K_\rho = 1/2$ , the corresponding spinless model has  $K = 1$  (cf. eq. (2.13)), i.e.  $g_2 = 0$ . Using eq.(2.20)  $H_\rho$  then transforms into

$$H_\rho = v_F \sum_k \{ (k - k_F) a_k^\dagger a_k + (-k - k_F) b_k^\dagger b_k \} + \frac{g_3}{2\pi\alpha} \sum_k (a_k^\dagger b_{k-2k_F} + b_k^\dagger a_{k+2k_F}) . \quad (3.5)$$

This form is easily diagonalized, and one finds an excitation spectrum for the spinless fermions of the form (noting that for half-filling  $k_F = \pi/2$ )

$$E_k = \pm [v_F^2 (k \pm \pi/2)^2 + \Delta^2]^{1/2} , \quad (3.6)$$

with a gap

$$\Delta = g_3/(2\pi\alpha) . \quad (3.7)$$

In the ground state all negative energy states are filled, all positive energy states are empty, and because of the gap the system then is an insulator. Note that the

fermion operators in (3.5) in fact create solitons in the  $\phi_\rho$  field, without affecting  $\phi_\sigma$ . At  $K_\rho \neq 1/2$ , the physical picture is not changed qualitatively, in particular there is still a gap in the charge excitation spectrum, however, the functional dependence is changed: in general, one has  $\Delta \propto g_3^\nu$ , with  $\nu = 1/(2 - 2K_\rho)$ .

The spin field  $\phi_\sigma$  is completely unaffected by the metal–insulator transition. Consequently, even the insulating state has a Pauli–like susceptibility, and long–range spin correlations of the type (2.48), with  $K_\rho = 0$ . This behavior is that of the one–dimensional antiferromagnetic Heisenberg model, which can be considered as a case of electrons localized on individual atoms. In the present case, the gap is typically much smaller than the bandwidth, and the localization length is therefore rather big. Nevertheless, the qualitative behavior of the correlations is the same.

We thus here have an example of a metal–insulator transition, occurring at constant particle density (half–filling) as a function of the interaction parameters. Approaching the transition from the metallic side, one has  $K_\rho \rightarrow 1$ ,  $u_\rho \rightarrow \text{const.}$ , and thus in particular the Drude weight of the conductivity remains finite and jumps discontinuously to zero as the transition line is crossed. This jump is nothing but the usual jump of the stiffness parameter (or “superfluid density”) of the Kosterlitz–Thouless transition. On the insulating side, the gap opens exponentially as a function of interaction strength, again the typical Kosterlitz–Thouless behavior.

One clearly would like to understand what happens if one is close to but not exactly half–filled. One thus adds a chemical potential term to the original model to obtain

$$H = H_0 + \sum_{i=1}^3 H_{int,i} - \mu \sum_{k,s} (a_{k,s}^\dagger a_{k,s} + b_{k,s}^\dagger b_{k,s}) . \quad (3.8)$$

In the bosonic description, the chemical potential term gives rise to a term proportional to  $\partial\phi_\rho/\partial x$ , which in turn, in the spinless fermion language of eq.(3.5) is equivalent to a chemical potential. For  $K_\rho = 1/2$ , the solution is still straightforward: as long as  $|\mu| < \Delta$ , the ground state is unchanged, but for  $\mu > \Delta$ , positive energy states start to be occupied (and similarly, for  $\mu < -\Delta$ , negative energy states are emptied). The number of extra carriers (i.e. the deviation of the carrier density from half–filling) varies as  $\delta n \propto \sqrt{|\mu| - \Delta}$ . The system is now metallic, and from eq.(3.6) one obtains the effective velocity of the charge modes as

$$u_\rho = \frac{v_F^2 |k_F - \pi/2|}{[v_F^2 (k_F - \pi/2)^2 + \Delta^2]^{1/2}} \quad (3.9)$$

In particular,  $u_\rho$  vanishes linearly as half–filling is approached. Thus, the Drude weight of the conductivity vanishes linearly as  $n \rightarrow 1$ .

If  $K_\rho \neq 1/2$  in eq.(3.4) there are additional interaction terms between the spinless fermions of eq.(3.5). However, in the vicinity of half–filling, these interactions can be eliminated from the problem [36, 37], and one has then for the effective parameter governing the low–energy physics  $K_\rho^* = 1/2$  in all cases, even if the original  $K_\rho$  was quite different from 1/2.

It should be emphasized here that  $K_\rho^* = 1/2$  is valid for  $n \rightarrow 1$ , but not for  $n = 1$ . In the latter case, there is a gap in the charge excitation spectrum due to the umklapp term (3.2), and the correlations of  $\phi_\rho$  become long ranged, i.e.  $K_\rho^* = 0$ . Close to half-filling, the asymptotic behavior of the charge part of correlation functions like (2.48) is essentially determined by the motion of the added carriers. Writing the density of carriers as  $\rho = |1 - n|$  one then expects a crossover of the form [36]

$$\langle \mathbf{S}(x) \cdot \mathbf{S}(0) \rangle \approx \cos(2k_F x) [1 + (\rho x)^2]^{-K_\rho/2} x^{-1} \ln^{1/2}(x) \quad (3.10)$$

for the  $2k_F$  part of the spin correlation function, and similarly for other correlation functions. Clearly, only for  $x \gg 1/\rho$  are the asymptotic power laws valid, whereas at intermediate distances  $1 \ll x \ll 1/\rho$  one has effectively  $K_\rho = 0$ . The form (3.10) provides a smooth crossover as  $n \rightarrow 1$ .

An interesting question is the sign of the charge carriers, especially close to the metal-insulator transition. The standard way to determine this, the sign of the Hall constant, is useless in a one-dimensional system. As an alternative, the thermopower can be used which is negative (positive) for electron (hole) conduction. In general, calculation of the thermopower is a nontrivial task, as the curvature of the bands plays an important role, and the approximate form of the Hamiltonian (2.30) is therefore insufficient. Moreover, both charge and spin entropies can play a role. However, close to the metal-insulator transition  $u_\rho \ll u_\sigma$ , and therefore the entropy of the charge degrees of freedom is much bigger than the spin entropy. As discussed above, the charge part of the Hamiltonian can be transformed into a model of massive fermions, with energy-momentum relation given by (3.6). At half-filling all negative energy states are filled, all positive energy states are empty. Doping with a concentration  $n^*$  of holes, some of the negative energy states become empty and only states with  $|k| > k_F^* \propto n^*$  are filled. Because of the vanishing interaction, a standard formula for the thermopower can be used [38] and gives

$$S = \frac{\pi^2 k_B^2 T}{6|e|} \frac{\Delta^2}{v^2 (k_F^*)^2 (v^2 (k_F^*)^2 + \Delta^2)^{1/2}}, \quad (3.11)$$

i.e. *approaching the metal-insulator transition from  $n < 1$ , the thermopower is hole-like*, whereas obviously far from the transition ( $n \ll 1$ ) it is electron-like. The exactly opposite behavior can be found for  $n > 1$ .

At zero temperature and away from half-filling, one has an infinite dc conductivity in this model. However, at finite temperature there is some probability to excite a carrier into a momentum state that makes umklapp scattering possible. One then expects a conductivity increasing exponentially at low temperature [37, 29].

For spinless fermions, a term like (3.1) cannot act, because of the Pauli principle. However, a term like

$$\int dx \{ \psi_+^\dagger(x) [\partial_x \psi_+^\dagger(x)] \psi_-(x) [\partial_x \psi_-(x)] + h.c. \} \approx \int dx \cos(4\phi(x)) \quad (3.12)$$

does produce umklapp scattering at half-filling and can give rise to a gap in the charge excitation spectrum if  $K \leq 1/4$  [39, 40, 41]. The metal-insulator transition



has properties analogous to that in the spin-1/2 case and has been studied in detail by Shankar [42]. A lattice model having this type of transition is the XXZ spin chain, which via a Jordan-Wigner transformation can be seen as a model of interacting spinless fermions.

### 3.2 Other commensurabilities

The umklapp operator (3.2) is effective at and near half-filling. One might wonder whether higher-order “commensurability”, i.e. in a third- or quarter-filled band, can also lead to insulating states, and at least intuitively it seems clear that this should be possible. On the other hand, for such cases, simple two-particle processes cannot be simultaneously momentum conserving (even modulo a reciprocal lattice vector) and only involve states near the Fermi energy. However, many-particle processes *induced by bare two-particle interactions do exist*: consider the case of a third-filled band ( $k_F = \pi/3$ ). In a first step then one has a (non-umklapp) process of the type  $(-\pi/3; -\pi/3) \rightarrow (-\pi; \pi/3)$ , with the particle at  $-\pi$  in a high-energy state at the band edge. In a second step one makes the transition  $(-\pi = \pi; -\pi/3) \rightarrow (\pi/3; \pi/3)$ . Umklapp here intervenes due to the identification of states at  $-\pi$  and  $\pi$ , and the final result is the transfer of three particles from  $-k_F$  to  $k_F$ . For weak two-particle interactions with an interaction matrix element  $g$  the effective matrix element  $g_u$  for this type of process is of order  $g^2/t$  (with bandwidth  $t$ ), but for stronger interactions it is hard to estimate. The generalization to bandfilling  $1/m$  (i.e.  $2/m$  particles per site) is straightforward: one transfers  $m$  particles from  $-k_F$  to  $k_F$ , with matrix element  $g_u \approx g^{m+1}/t^m$ .

To take the existence of this type of processes into account in the original continuum description, one adds a term

$$H_u = g_u \int dx \{[\psi_-^\dagger(x)]^m [\psi_+(x)]^m + h.c.\} , \quad (3.13)$$

where the product of many fermion operators at one site is to be understood as point-split, and the spin summation is implied. In the bosonic language, this term translates into

$$H_u = g_u \int dx \{O_{CDW}(x)^m + h.c.\} \quad (3.14)$$

$$\approx g_u \int dx \cos^m(\sqrt{2}\phi_\sigma(x)) \cos(\sqrt{2}m\phi_\rho(x)) . \quad (3.15)$$

There are now two physically rather different cases, according to whether  $n$  is even or odd. Consider first the even case. Then the  $\cos^m(\sqrt{2}\phi_\sigma(x))$  term can be expanded, and the lowest-order (most relevant in the renormalization group sense) comes from the constant in this expansion, e.g. the effective  $H_u$  is

$$H_u \approx g_u \int dx \cos(\sqrt{2}m\phi_\rho(x)) . \quad (3.16)$$

After a simple unitary transformation rescaling  $\phi_\rho$ , we have now a problem formally identical to the half-filled case. At filling exactly equal to  $1/m$  we thus have an insulating or a metallic phase, with the metallic state stable for  $K_\rho \geq 4/m^2$ , and  $K_\rho^* = 4/m^2, u_\rho^* = \text{const.}$  at the metal-insulator transition. For  $m > 2$  the condition for the existence of an insulating state,  $K_\rho < 4/m^2$ , usually requires strongly repulsive interactions, and even then can not always be satisfied: e.g. for the Hubbard model,  $K_\rho > 1/2$  even for infinitely strong repulsion. In the insulating state,  $\phi_\rho$  has only small oscillations around a fixed average value, and thus the effective  $K_\rho$  is zero. We then have long-range charge density wave order at wavevector  $4k_F$ , but still the spin-spin correlations typical of the one-dimensional antiferromagnetic Heisenberg model (cf. eq. (2.48)). We note that the solitons in this case have a jump in  $\phi_\rho$  of  $\sqrt{2}\pi/m$ , and thus carry charge  $2/m$ . As in the half-filled case, the magnetic properties are largely independent on whether one is in the insulating or metallic state.

Varying the particle density at constant  $K_\rho < 4/m^2$ , one recovers behavior similar to the nearly-half-filled case above: as  $n \rightarrow 2/m$  one has  $u_\rho \rightarrow 0$  and  $K_\rho \rightarrow 2/m^2$ . Of course, for  $m = 2$  we recover precisely the results of the preceding section.

Things are a bit more complicated if  $m$  is odd. In this case the most relevant term in  $H_u$  takes the form

$$H_u \approx g_u \int dx \cos(\sqrt{2}\phi_\sigma(x)) \cos(\sqrt{2}m\phi_\rho(x)) \ , \quad (3.17)$$

e.g. spin and charge degrees of freedom are coupled. The scaling dimension of this operator is  $(1 + m^2 K_\rho)/2$ , and consequently this operator is relevant and produces a gap if  $K_\rho < 3/m^2$ . The insulating state is characterized by a large effective  $g_u$ , and consequently, from (3.17) one expects both  $\phi_\rho$  and  $\phi_\sigma$  to oscillate around stable equilibrium positions, i.e. there is a gap in both the charge and the spin excitations, and the ground state is non-magnetic and one has  $2k_F$  CDW ordering (in contrast to the paramagnetic ground state and  $4k_F$  CDW found for  $m$  even), There are now separate soliton-like excitations for charge and spin, carrying charge  $2/m$  and spin  $1/2$ , respectively.

In a particular case, an exact solution of the odd- $m$  problem can be given: assume  $g_1 = 0$  (which anyway is the fixed-point value for repulsive interactions). Then, after the unitary transformation  $\phi_\rho \rightarrow \phi_\rho/m$ , the total Hamiltonian, e.g. the sum of (2.30) and (3.17) becomes

$$\begin{aligned} H = & \int dx \left[ \frac{\pi u_\rho K_\rho m^2}{2} \Pi_\rho^2 + \frac{u_\rho}{2\pi K_\rho m^2} (\partial_x \phi_\rho)^2 \right] \\ & + \int dx \left[ \frac{\pi u_\sigma}{2} \Pi_\sigma^2 + \frac{u_\sigma}{2\pi} (\partial_x \phi_\sigma)^2 \right] \\ & + g_u \int dx \cos(\sqrt{2}\phi_\sigma(x)) \cos(\sqrt{2}\phi_\rho(x)) \ , \end{aligned} \quad (3.18)$$

The  $g_u$ -term now has exactly the form of the  $2k_F$  CDW operator (2.45), i.e. it is bilinear in fermion operators. Moreover, for  $K_\rho = 1/m^2$  and  $u_\rho = u_\sigma = u$ , the

first two terms in (3.18) represent free spin-1/2 fermions, e.g. in this case the full Hamiltonian is in fact the spin-1/2 version of (3.5):

$$\begin{aligned}
H = & v_F \sum_{k,s} \{ (k - k_F) a_{k,s}^\dagger a_{k,s} + (-k - k_F) b_{k,s}^\dagger b_{k,s} \} \\
& + g_u \sum_{k,s} (a_{k,s}^\dagger b_{k-2k_F,s} + b_{k,s}^\dagger a_{k+2k_F,s}) .
\end{aligned} \tag{3.19}$$

This form is of course easily diagonalized, and, as expected one has a gap both in the charge and in the spin excitations. In this particular case these gaps are equal, but generally, e.g. for  $K_\rho \neq 1/m^2$ , this will not be the case.

If one is away from filling  $1/m$ , an additional chemical potential term appears in (3.19), and either states above the gap get filled or states below the gap become empty. This is very similar to the nearly-half-filled case. Because we have effectively noninteracting electrons in (3.19), one still has  $K_\rho = 1/m^2$ , and  $u_\rho \propto |n - 2/m|$ . However, and *contrary to the case of  $m$  even*, now the spin velocity shows critical behavior:  $u_\sigma \propto |n - 2/m|$ , leading in particular to a diverging spin susceptibility.

This behavior is however not generic: if  $K_\rho$  deviates only slightly from  $1/m^2$ , or one of the other solvability conditions is not satisfied, there are interaction terms in addition to the free fermion Hamiltonian (3.19). Close to filling  $1/m$  there are very few extra fermions, compared to  $n = 2/m$ . However, and contrary to the spinless case relevant for  $m$  even, interactions do have dramatic effects on spin-1/2 fermions even in the very dilute limit. In fact, as long as the interaction is not long-ranged, for sufficiently high dilution (more precisely, if the interparticle distance is bigger than the scattering length), the precise form of the interaction matrix element is expected to be unimportant. One can then take over exact results available for the one dimensional Hubbard model in the dilute limit (see sec. 4.3.1). In particular, if the interactions added to (3.19) are repulsive (for  $u_\rho = u_\sigma$  this corresponds to  $K_\rho < 1/m^2$ ), one has  $u_\rho \propto |n - 2/m|$ , but now  $K_\rho^* = 1/(2m^2)$ , and in particular  $u_\sigma \propto (n - 2/m)^2$ , i.e. there is a very strong divergence of the spin susceptibility. On the other hand, for attractive extra interactions in (3.19), a spin gap opens close to  $n = 2/m$ , and one then has  $u_\rho \propto |n - 2/m|$ ,  $K_\rho^* = 1/m^2$ . A summary of the different types of critical behavior of the Luttinger liquid parameters  $K_\rho$  and  $u_{\rho,\sigma}$  and of some derived physical quantities is given in table 1.

The differences between even and odd filling fraction  $m$  may a priori seem surprising. However, there is a simple explanation, illustrated in figure 1. Assume a lattice model with strong finite-range repulsion. Then, for  $m$  even, the ground state will essentially be a regular sequence of atoms, with one fermion every  $m/2$  lattice sites. The spins of the fermions will interact via an exchange term that is a generalization of the usual  $t^2/U$  term, so that in fact we have a  $4k_F$  charge density wave forming an antiferromagnetic spin chain. This is exactly the ground state we derived from (3.16).

On the other hand, for odd  $m$  a completely equidistant arrangement is not possible, as illustrated in fig.1 for  $m = 3$ . In fact, a band filling of  $1/m$  corresponds

Table 1: Critical behavior of the different metal–insulator transitions considered in this paper. The transition is approached from the metallic side. For additional explanations on the last column see the text.

	$n = 2/m$	$n = 2/m$	$n \rightarrow 2/m$	$n \rightarrow 2/m$
	$K_\rho \rightarrow K_\rho^*$	$K_\rho \rightarrow K_\rho^*$	$K_\rho = \text{const.}$	$K_\rho = \text{const.}$
	$m \text{ even}$	$m \text{ odd}$	$m \text{ even}$	$m \text{ odd}$
$K_\rho^*$	$4/m^2$	$3/m^2$	$2/m^2$	$1/(2m^2)$
$u_\rho$	const.	const.	$ n - 1/m $	$ n - 1/m $
$u_\sigma$	const.	const.	const.	$(n - 1/m)^2$
$\gamma$	const.	const.	$1/ n - 1/m $	$1/ n - 1/m $
$\chi$	const.	const.	const.	$1/(n - 1/m)^2$
$R_W$	const.	const.	0	2

to an average  $2/m$  fermions per site. Consequently, the ground state arrangement is an alternation of short and long “bonds”, and one has a  $2k_F$  CDW. In addition, there is of course an alternation of the exchange constants from long to short bonds, and such an alternation is well-known to introduce a gap in the spin excitation spectrum. We thus again explain the behavior derived from (3.17).

The above considerations can be extended to obtain a lower bound on the correlation exponent  $K_\rho$  in a certain class of models: consider a lattice model with a finite range interaction of the form

$$H_{int} = \sum_{i,m \geq 0} V_m n_i n_{i+m} . \quad (3.20)$$

Let us assume further that  $V_m = 0$  for  $m \geq m_0$ , where  $m_0$  thus specifies the range of the interaction ( $m_0 = 1$  and  $2$  for the Hubbard and extended Hubbard models discussed below). I will further assume strictly repulsive interactions, e.g.  $V_m > V_{m+1}$ . Then, in the strong coupling limit it is quite clear that the longest interparticle distance in a stable structure is  $m_0$ . In particular, the most dilute stable structure has just one particle every  $m_0$  sites, i.e. it has period  $m_0$ , and commensurate states with period larger than  $m_0$  are not stable (stability here implies the existence of a gap in the charge excitation spectrum). In the continuum limit, a structure with period say  $m_0 + 1$  can be stabilized by a term  $\approx \cos(\sqrt{8}(m_0 + 1)\phi_\rho)$ , which has scaling dimension  $x_{m_0+1} = 2(m_0 + 1)^2 K_\rho$ . This term will generate a stable commensurate structure if it is relevant, i.e. if  $x_{m_0+1} \leq 2$ . On the other hand, for it *not* to create a stable commensurate structure (as expected), one needs  $x_{m_0+1} > 2$ . Thus, for purely repulsive models with interaction of the form (3.20) and range  $m_0$  one has the limit

$$K_\rho > \frac{1}{(m_0 + 1)^2} . \quad (3.21)$$

The assumption we have made here is that quite generally  $K_\rho$  decreases if the interaction term (3.20) is increased by applying a overall scale factor that is larger than unity. The limit (3.21) is satisfied for the lattice models discussed in the next section.

## 4 The Hubbard model in one dimension

### 4.1 The Hamiltonian and its symmetries

The Hubbard model is the prototypical model used for the description of correlated fermions in a large variety of circumstances, ranging from high- $T_c$  superconductors to heavy fermion compounds and organic conductors. In spite of its apparent simplicity, there is still no general solution, or even a consensus on its fundamental properties. Notable exceptions are the cases of one and infinite dimensions [43, 44]. In particular, in one dimension an exact solution is available. This solution gives exact energies of the ground state and all the excited states in terms of the solution of a system of coupled nonlinear equations. On the other hand, the corresponding wavefunctions have a form so complicated that the explicit calculation of matrix elements, correlation functions and other physical quantities has remained impossible so far. In the following sections I shall describe in some detail the energy spectrum obtained from the exact solution. Subsequently, I will show how the knowledge of the energy spectrum can be combined with the results of the preceding two chapters to obtain a rather detailed picture of the low-energy properties, in particular of correlation functions, and of the metal insulator transition.

The Hamiltonian in one dimension has the well-known form

$$H = -t \sum_{i,s} (c_{i,s}^\dagger c_{i+1,s} + c_{i+1,s}^\dagger c_{i,s}) + U \sum_i n_{i,\uparrow} n_{i,\downarrow} \quad , \quad (4.1)$$

where  $c_{i,s}$  is the fermion annihilation operator on site  $i$  with spin  $s$ ,  $n_{i,s}$  is the corresponding number operator, and the sum is over the  $L$  sites of a one-dimensional chain with periodic boundary conditions.

The model has *two* global  $SU(2)$  symmetries [45, 46, 47]: the first is the well-known spin rotation invariance, with generators

$$\zeta = \sum_{i=1}^L c_{i,\uparrow}^\dagger c_{i,\downarrow}, \quad \zeta^\dagger = (\zeta)^\dagger, \quad \zeta_z = \frac{1}{2} \sum_{i=1}^L (n_{i,\downarrow} - n_{i,\uparrow}) \quad . \quad (4.2)$$

The second type of symmetry is particular to the Hubbard model and relates sectors of different particle numbers. Its generators are

$$\eta = \sum_{i=1}^L (-1)^i c_{i,\uparrow}^\dagger c_{i,\downarrow}, \quad \eta^\dagger = (\eta)^\dagger, \quad \eta_z = \frac{1}{2} \sum_{i=1}^L (n_{i,\downarrow} + n_{i,\uparrow}) - \frac{L}{2} \quad . \quad (4.3)$$

The total symmetry thus is  $SU(2) \times SU(2) \simeq SO(4)$ . One should notice that more complicated interactions, e.g. involving further neighbors, will conserve the spin rotation invariance but in general not the “charge”  $SU(2)$  invariance (4.3). Rather, this second symmetry will become the standard global  $U(1)$  invariance associated with particle number conservation. It is nevertheless possible to construct particular types of further-neighbor interactions which do conserve the full  $SU(2) \times SU(2)$  invariance.

## 4.2 The exact solution: ground state and excitations

The exact wavefunctions of the one-dimensional Hubbard model for  $N$  particles are superpositions of plane waves characterized by a set  $\{k_j\}$  of momenta [3]. The allowed values of  $k_j$  are obtained from the solution of the coupled set of nonlinear equations

$$e^{ik_j L} = \prod_{\alpha=1}^M e\left(\frac{4(\sin k_j - \lambda_\alpha)}{U}\right) \quad (4.4)$$

$$\prod_{j=1}^N e\left(\frac{4(\lambda_\alpha - \sin k_j)}{U}\right) = - \prod_{\beta=1}^M e\left(\frac{2(\lambda_\alpha - \lambda_\beta)}{U}\right) , \quad (4.5)$$

Here  $M$  is the number of down-spin electrons ( $M \leq N/2$ ) and  $e(x) = (x+i)/(x-i)$ . The  $\lambda_\alpha$  are parameters characterizing the spin dynamics. We note that in general, both the  $k_j$ 's and the  $\lambda$ 's are allowed to be complex. The energy and momentum of a state are

$$E = -2t \sum_{j=1}^N \cos k_j \quad , \quad P = \sum_{j=1}^N k_j . \quad (4.6)$$

### 4.2.1 Solutions of the Bethe ansatz equations

The determination of all the solutions of eqs. (4.4, 4.5) is not easy. It has recently been shown (under certain assumptions) that these equations do indeed give all the “lowest weight” (with respect to  $SU(2) \times SU(2)$ ) eigenstates of the Hubbard model, i.e. all states satisfying  $\eta|\psi\rangle = \zeta|\psi\rangle = 0$ . The complete set of eigenstates then is obtained acting repeatedly with  $\eta^\dagger$  or  $\zeta^\dagger$  on  $|\psi\rangle$  [48]. Here I will limit myself to the ground state and to the low-lying elementary excitations. These questions have been investigated in some detail [49, 50, 51], however, the finite chain data presented below seem to be quite useful in understanding the nature of the excitations, and I therefore discuss them in detail.

If both the  $k$ 's and the  $\lambda$ 's are all real, only the phases in (4.4, 4.5) have to be determined. Taking the logarithm of these equations, one finds

$$Lk_j = 2\pi I_j + 2 \sum_{\alpha=1}^M \arctan[4(\lambda_\alpha - \sin k_j)/U] \quad (4.7)$$

$$2 \sum_{j=1}^N \arctan[4(\lambda_\alpha - \sin k_j)/U] = 2\pi J_\alpha + 2 \sum_{\beta=1}^M \arctan[2(\lambda_\alpha - \lambda_\beta)/U] . \quad (4.8)$$

The quantum numbers  $\{I_j\}$  are all distinct from each other and are integers if  $M$  is even and half-odd integers (HOI, i.e. of the form  $1/2, 3/2, \dots$ ) if  $M$  is odd, and are only defined modulo  $L$ . Similarly, the set  $\{J_\alpha\}$  are all distinct and are integers if  $N - M$  is odd and HOI if  $N - M$  is even. Moreover, there is the restriction

$$|J_\alpha| < (N - M + 1)/2 . \quad (4.9)$$

Summing (4.7) over  $j$  and (4.8) over  $\alpha$ , the total momentum is found as

$$P = \frac{2\pi}{L} \left( \sum_{j=1}^N I_j + \sum_{\alpha=1}^M J_\alpha \right) . \quad (4.10)$$

**Ground state.** The ground state is nondegenerate only if  $N$  is of the form  $4\nu + 2$  ( $\nu$  integer): obviously, if  $N$  is odd, the ground state has (at least) spin  $1/2$ . Further, if  $N$  is an integer multiple of 4 the noninteracting ground state has a sixfold degeneracy, and in the interacting case the ground state turns out to be a spin triplet. In the following I shall restrict myself to the case of  $N = N_0 = 4\nu + 2$ , i.e. the ground state is nondegenerate (in the following,  $N_0$  will denote the particle number in the ground state). The ground state then is a singlet, with  $M = N_0/2$ , i.e.  $M$  is odd. The allowed values of the  $J$ 's range from  $-(N_0/2 - 1)/2$  to  $(N_0/2 - 1)/2$ . There are exactly  $N_0/2$  such integers, i.e. all the  $J$ 's are fixed. The  $I$ 's are consecutive between  $-(N_0 - 1)/2$  and  $(N_0 - 1)/2$ , i.e.

$$\{I_j\} = \{-(N_0 - 1)/2, \dots, (N_0 - 1)/2\} , \quad (4.11)$$

$$\{J_\alpha\} = \{-(N_0/2 - 1)/2, \dots, (N_0/2 - 1)/2\} . \quad (4.12)$$

In the thermodynamic limit  $L \rightarrow \infty$  the distance between consecutive  $k$ 's or  $\lambda$ 's decrease like  $1/L$ , and one can then find linear integral equations for the density of  $k$ 's and  $\lambda$ 's on the real axis. Numerical results for the ground state energy as a function of particle density and  $U$  have been given by Shiba [49].

At half-filling, there is a gap in the charge excitations [3], and only spin excitations ( the “ $2k_F$ ” triplet and singlet states below) are gapless. In particular, a finite energy is required to add or take out a particle. On the other hand, away from half-filling, both charge and spin excitations are massless.

**“ $4k_F$ ” singlet states.** Excited states are obtained by varying the quantum numbers. The first possibility, giving rise to excited singlet states, is obtained by removing one of the  $I$ 's from the ground state sequence (4.11) and adding a “new”  $I$ :

$$\begin{aligned} \{I_j\} &= \{-(N_0 - 1)/2, \dots, -(N_0 - 1)/2 + i_0 - 1, \\ &\quad -(N_0 - 1)/2 + i_0 + 1, \dots, (N_0 - 1)/2, I_0\} , \\ \{J_\alpha\} &= \{-(N_0/2 - 1)/2, \dots, (N_0/2 - 1)/2\} , \end{aligned} \quad (4.13)$$

where  $|I_0| > (N_0 - 1)/2$ . This is a two-parameter family of excited states, called (somewhat misleadingly) “particle-hole excitation” by Coll. To understand the excited states, we shall in the following consider systems of finite size, rather than taking the thermodynamic limit directly. It should however be quite evident how spectra like those of fig.2 develop into a true continuum in the thermodynamic limit. In fig.2 we show numerical results for the energy-momentum spectrum of the states (4.13) for a chain of 40 sites. The same states with  $k \rightarrow -k$  are obtained using negative

$I_0$ . One notices a sharp minimum in the excitation energy at  $k/\pi = 1.1(1.7) = 4k_F$  (this is why I call these excitations “ $4k_F$ ” singlets). In the thermodynamic limit, the gap at  $4k_F$  vanishes. These excitations are at the origin of the power-law behavior in the density-density correlation function (2.47) around  $4k_F$ . Moreover, in the bosonization formalism, the  $4k_F$  density correlations are entirely determined by the charge ( $\phi_\rho$ ) modes. Consequently, we identify the charge velocity  $u_\rho$  as the slope of the excitation spectrum of fig.2 at  $k = 0$ . Finally, we notice that the total number of states in this branch decreases as one approaches half-filling, and that this branch disappears altogether at half-filling. In fact, at half-filling, charge excitations have a gap and are described by solutions with complex  $k$ 's [52].

**“ $2k_F$ ” triplet and singlet states.** Excitations of the  $J$ 's with all  $\lambda$ 's and  $k$ 's real are only possible if  $M < N/2$ . The simplest excitations of this type are obtained considering  $M = N/2 - 1$  which has total spin  $S = 1$  (triplet). Now the restriction (4.9) allows  $N/2 + 1$  different  $J$ 's, i.e. we have two free parameters (the “holes” in the  $J$ -sequence), leading to sequences of quantum numbers of the form

$$\begin{aligned} \{I_j\} &= \{-N_0/2 + 1, \dots, N_0/2\} \ , \\ J_1 &= -N_0/4 + \delta_{\alpha_1,1} \ , \\ J_\alpha &= J_{\alpha-1} + 1 + \delta_{\alpha,\alpha_1} + \delta_{\alpha,\alpha_2} \quad (\alpha = 2, \dots, M) \ , \end{aligned} \tag{4.14}$$

where  $1 \leq \alpha_1 < \alpha_2 \leq M$ , and  $\delta_{\alpha,\beta}$  is the usual Kronecker symbol. Numerical results for this type of excitations are shown in fig.3. Corresponding states with negative  $k$  are obtained shifting the  $\{I_j\}$  in (4.14) by one unit to the left. There now is a sharp minimum at  $k/\pi = 0.55 = 2k_F$ , the gap again vanishing in the thermodynamic limit. In the long-wavelength limit, these states are the only spin-carrying excitations at constant particle number, so that the slope of the spectrum at  $k = 0$  is equal to the spin velocity of the bosonized model. The low-energy excitations around  $2k_F$  are responsible for the spin contribution to the  $2k_F$  spin-spin correlations. As in fig.2, the structure of the excitations doesn't change much between weak and strong correlations, however, the energy scale does. In fact, the lowering of the energy scale in going to strong correlations corresponds to the lowering of the exchange energy ( $\approx 4t^2/U$ ) in the strong correlation limit. The results of fig.3 show apparent gaps at  $2k_F$  and  $4k_F$ . These are finite size effects: in the thermodynamic limit  $L \rightarrow \infty$  the gaps vary like  $1/L$ , and simultaneously the spectra develop into a continuum.

Together with the triplet excitations (4.14) there are also singlet states ( $M = N_0/2$ ), which are obtained by having one pair of complex conjugate  $\lambda$ 's among the solutions to the original equations (4.4, 4.5). The energies of these states are shown by triangles in fig.2. It is remarkable that these states are nearly degenerate with the triplet states and in fact become exactly degenerate in the thermodynamic limit.

The existence of singlets and triplets with the same energy shows that these states are in fact the combination of two *noninteracting spin-1/2 objects*, commonly



called *spinons*. Of course, because of total spin conservation, these objects can only be excited in pairs as long as one keeps the total number of particles fixed.

**Added particle.** Adding one particle to the  $4\nu + 2$  ground state and leaving  $M$  unchanged, the  $I$ 's and the  $J$ 's are HOI. There are now  $M + 1$  allowed values for the  $M$  distinct  $J$ 's, and the low-energy states then are parameterized by

$$\begin{aligned} \{I_j\} &= \{-(N_0 - 1)/2, \dots, (N_0 - 1)/2, I_0\} \ , \\ J_1 &= -M/2 + \delta_{\alpha_1, 1} \ , \\ J_\alpha &= J_{\alpha-1} + 1 + \delta_{\alpha, \alpha_1} \quad (\alpha = 2, \dots, M) \ , \end{aligned} \tag{4.15}$$

where  $|I_0| > (N_0 - 1)/2$ , and  $1 \leq \alpha_1 \leq M$ . Corresponding spectra for different bandfillings are shown in fig.4 for  $I_0 > 0$ . The symmetric spectra with negative  $k$  are again obtained using  $I_0 < 0$ . The state of minimal excitation energy has momentum  $k_F$ , as in the noninteracting case. The shallow arches in fig.4 correspond to varying  $\alpha_1$ , and are in fact of the same shape as the lowest branch (from  $k = 0.05\pi$  to  $k = 0.55\pi$ ) in fig.3, i.e. they correspond to *single-spinon* excitations. Close to  $k_F$  the energy of these states varies as  $u_\sigma(k - k_F)$ . On the other hand, varying  $I_0$ , one goes from one arc to the next, and the corresponding excitation energy (the upper limit of the quasi-continuum) varies as  $u_\rho(k - k_F)$ . One also sees that going from one arc to the next in fig.4 (i.e. increasing  $I_0$ ) the shape of an individual arc is basically unchanged. Varying  $I_0$  corresponds to a variation of the momentum of the added particle, and the figure thus shows that the total energy of a state is just the sum of the spinon energy and the “charge” energy associated with the added particle. One thus sees that *charge and spin degrees of freedom do not interact*. This is certainly in agreement with the predictions of the bosonization formalism, however, the fact that spin and charge separate even in highly excited states is special to the Hubbard model (a priori, the bosonized theory can only be expected to be an effective low-energy theory for the Hubbard and other lattice models).

Another notable fact in fig.4 is the number of available states as  $I_0$  is varied: for  $N_0 = 14, 22$ , and  $30$  there are respectively 13, 9, and 5 spinon arches. This means that without exciting the spins there are 26, 18, and 10 states for the extra particle available (counting states at negative  $k$ ), i.e. the  $I_0$  branch stops at  $k = \pi - k_F$ , rather than at  $k = \pi$  as in a noninteracting system. The explanation of this fact is rather straightforward for large  $U$  when double occupancy of sites is forbidden: in a system with  $L$  sites and  $N_0$  electrons, there are only  $L - N_0$  sites available at low energies. These states then form the “band” in fig.4. There are of course states involving doubly occupied sites, however these are separated from the continuum of fig.4 by a gap (these states are solutions of (4.4, 4.5) with complex  $k$ 's [52]). This separation of states occurs for any, even very small  $U$ , and can actually be shown by a perturbative argument [53].

**Added hole.** Finally, let us consider states with one hole in the  $4\nu + 2$  groundstate ( $N = N_0 - 1, M = (N - 1)/2$ ). Then both the  $I$ 's and the  $J$ 's are integers. The energy is minimized choosing consecutive  $I$ 's between  $-(N - 1)/2$  and  $(N - 1)/2$ , but there are  $M + 1$  possibilities for the  $M$   $J$ 's. States corresponding to the sequence

$$\begin{aligned} \{I_j\} &= \{-(N - 1)/2, \dots, (N - 1)/2\} \ , \\ J_1 &= -M/2 + \delta_{\alpha_1, 1} \ , \\ J_\alpha &= J_{\alpha-1} + 1 + \delta_{\alpha_1, \alpha} \quad (\alpha = 2, \dots, M) \end{aligned} \quad (4.16)$$

are shown as the lowest arc between  $k = -0.25\pi$  and  $k = 0.25\pi$ . This is a one-spinon branch, this state having necessarily  $S = 1/2$ , with velocity  $u_\sigma$ . One can of course also create a hole in the sequence of  $I$ 's. The energy spectrum for the quantum numbers

$$\begin{aligned} I_1 &= -(N + 1)/2 + \delta_{j_1, 1} \\ I_j &= I_{j-1} + 1 + \delta_{j_1, j} \quad (j = 2, \dots, N) \end{aligned} \quad (4.17)$$

$$\begin{aligned} J_1 &= -M/2 + \delta_{\alpha_1, 1} \ , \\ J_\alpha &= J_{\alpha-1} + 1 + \delta_{\alpha_1, \alpha} \quad (\alpha = 2, \dots, M) \end{aligned} \quad (4.18)$$

(where the free parameters obey  $1 \leq j_1 \leq N, 1 \leq \alpha_1 \leq M$ ) is also shown in fig.5. Similarly to fig.4, one notices that varying the ‘‘charge’’ quantum number  $j_1$  one creates a branch with velocity  $u_\rho$ .

## 4.3 Low energy properties of the Hubbard model

### 4.3.1 Luttinger liquid parameters

In a weakly interacting system the coefficients  $K_\rho$  and  $u_\nu$  can be determined perturbatively. For example, for the Hubbard model one finds

$$K_\rho = 1 - U/(\pi v_F) + \dots \ , \quad (4.19)$$

where  $v_F = 2t \sin(\pi n/2)$  is the Fermi velocity for  $n$  particles per site. For larger  $U$  higher operators appear in the continuum Hamiltonian (2.30), e.g. higher derivatives of the fields or cosines of multiples of  $\sqrt{8}\phi_\sigma$ . These operators are irrelevant, i.e. they renormalized to zero and do not qualitatively change the long-distance properties, but they do lead to nontrivial corrections to the coefficients  $u_\nu, K_\rho$ . In principle these corrections can be treated order by order in perturbation theory. However, this approach is obviously unpractical for large  $U$ , and moreover it is at least possible that perturbation theory is not convergent. To obtain the physical properties for arbitrary  $U$  a different approach is therefore necessary.

I note two points: (i) in the small- $U$  perturbative regime, interactions renormalize to the weak-coupling fixed point  $g_1^* = 0, K_\sigma^* = 1$ ; (ii) the exact solution [3] does not show any singular behavior at nonzero  $U$ , i.e. large  $U$  and small  $U$  are the

same phase of the model, so that the long-range behavior even of the large  $U$  case is determined by the fixed point  $g_1^* = 0$ . Thus, the low energy properties of the model are still determined by the three parameters  $u_{\rho,\sigma}$  and  $K_\rho$ .

The velocities  $u_{\rho,\sigma}$  can be obtained from the long wavelength limit of the “ $4k_F$ ” and “ $2k_F$ ” excitations discussed above. In the thermodynamic limit the corresponding excitation energies are easily found from the numerical solution of a linear integral equation [50]. Results are shown in fig.6 for various values of  $U/t$ . Note that for  $U = 0$  one has  $u_\rho = u_\sigma = 2t \sin(\pi n/2)$ , whereas for  $U \rightarrow \infty$   $u_\rho = 2t \sin(\pi n)$ ,  $u_\sigma = (2\pi t^2/U)(1 - \sin(2\pi n)/(2\pi n))$ . In the noninteracting case  $u_\sigma \propto n$  for small  $n$ , but for *any* positive  $U$   $u_\sigma \propto n^2$ . The Wilson ratio, eq.(2.38), obtained from the velocities is shown in fig.6. For  $U = 0$  one has  $R_W = 1$ , whereas for  $U \rightarrow \infty$   $R_W = 2$  for  $n \neq 1$ .

To obtain the parameter  $K_\rho$  from the exact solution note that the gradient of the phase field  $\phi_\rho$  is proportional to the particle density, and in particular a constant slope of  $\phi_\rho$  represents a change of total particle number. Consequently, the coefficient  $u_\rho/K_\rho$  in eq. (2.31) is proportional to the variation of the ground state energy  $E_0$  with particle number [18]:

$$\frac{1}{L} \frac{\partial^2 E_0(n)}{\partial n^2} = \frac{\pi u_\rho}{2 K_\rho} = \frac{1}{n^2 \kappa} . \quad (4.20)$$

Equation (4.20) now allows the direct determination of  $K_\rho$ :  $E_0(n)$  can be obtained solving (numerically) Lieb and Wu’s [3] integral equation, and  $u_\rho$  is already known. The results for  $K_\rho$  as a function of particle density are shown in fig.8 for different values of  $U/t$ . For small  $U$  one finds in all cases agreement with the perturbative expression, eq. (4.19), whereas for large  $U$   $K_\rho \rightarrow 1/2$ . The limiting behavior for large  $U$  can be understood noting that for  $U = \infty$  the charge dynamics of the system can be described by noninteracting *spinless* fermions (the hard-core constraint then is satisfied by the Pauli principle) with  $k_F$  replaced by  $2k_F$ . Consequently one finds a contribution proportional to  $\cos(4k_F x)x^{-2}$  in the density-density correlation function, which from eq. (2.47) implies  $K_\rho = 1/2$ . One then finds an asymptotic decay like  $\cos(2k_F x)x^{-3/2} \ln^{1/2}(x)$  for the spin-spin correlations, eq.(2.48), and an exponent  $\delta = 1/8$  in the momentum distribution function. The result  $\delta = 1/8$  has also been found by Anderson and Ren [54], and by Parola and Sorella [55]. Ogata and Shiba’s numerical results [17] are quite close to these exact values.

As is apparent from fig.8, the strong-coupling value  $K_\rho = 1/2$  is also reached in the limits  $n \rightarrow 0, 1$  for *any positive*  $U$ . For  $n \rightarrow 0$  this behavior is easily understood: the effective interaction parameter is  $U/v_F$ , but  $v_F$  goes to zero in the low-density limit (corresponding to the diverging density of states). The limit  $n \rightarrow 1$  is more subtle: in this case nearly every site is singly occupied, with a very low density of holes. The only important interaction then is the short range repulsion between holes, which can be approximated by treating the *holes* as a gas of spinless noninteracting fermions. Using (4.20), one then again finds  $K_\rho = 1/2$ .

We note that in the whole parameter region, as long as the interaction is repulsive one always has  $K_\rho < 1$ , which means that magnetic fluctuations are enhanced over the noninteracting case. On the other hand, superconducting pairing is always suppressed.

The results of fig.8 are valid for  $n \rightarrow 1$ , but not for  $n = 1$ . In the latter case, there is a gap in the charge excitation spectrum, as expected from the umklapp term (3.2), and the correlations of  $\phi_\rho$  become long ranged ( $K_{\rho,eff} = 0$ ). Close to half-filling, the asymptotic behavior of correlation functions then exhibits a crossover behavior from half-filled-like behavior at short distances to the general form at long distances, as discusses in sec.3.1 above (see in particular eq. (3.10).

Results equivalent to the present ones can be obtained using the conformal invariance of the Hubbard model [56, 57]. These results have subsequently be generalized to the case with an applied magnetic field [58].

### 4.3.2 Transport properties

The exact solution of Lieb and Wu can also be combined with the long-wavelength effective Hamiltonian (2.30) to obtain some information on the frequency-dependent conductivity  $\sigma(\omega)$ . On the one hand, from eq. (2.39) there is a delta function peak at zero frequency of weight  $2K_\rho u_\rho$ . On the other hand, the total oscillator strength is proportional to the kinetic energy [59]:

$$\sigma_{tot} = \int_{-\infty}^{\infty} \sigma(\omega) d\omega = -\pi \langle H_{kin} \rangle / L . \quad (4.21)$$

Thus, both the weight of the dc peak and the relative weight of the dc peak in the total conductivity can be obtained and are plotted in fig.9. As expected, far from half-filling, all the weight in  $\sigma_{tot}$  is in the dc peak. For exactly half-filling the dc conductivity vanishes, due to the existence of a gap  $\Delta_c$  for charge excitations created by umklapp scattering, and all the weight is at  $\omega > \Delta_c$ . Fig.2 then shows that as  $n \rightarrow 1$  umklapp scattering progressively transfers weight from zero to high frequency. The crossover is very sharp for small or large  $U$ , but rather smooth in intermediate cases ( $U/t \approx 16$ ). This nonmonotonic behavior as a function of  $U$  can be understood noting that initially with increasing  $U$  umklapp scattering plays an increasingly important role. Beyond  $U/t \approx 16$ , however, the spinless-fermion picture becomes more and more appropriate, and at  $U = \infty$  one again has all the weight in the dc peak. The linear vanishing of  $\sigma_0$  as  $n \rightarrow 1$  implies a linear variation of the ratio  $n/m^*$  with “doping”. By the thermopower-argument of sec.3.1 carriers are hole-like for  $n < 1$ , and electron-like for  $n > 1$ , provided one is close to the transition. The thermopower of the one-dimensional Hubbard model as well as the rather subtle crossover occurring in the vicinity of the critical point  $n = 1, U = 0$  have been analyzed in detail recently [60, 61].

### 4.3.3 Spin–charge separation

The Hubbard model also provides a rather straightforward interpretation of the spin–charge separation discussed above. Consider a piece of a Hubbard chain with a half–filled band. Then for strong  $U$  there will be no doubly–occupied sites, and because of the strong short–range antiferromagnetic order the typical local configuration will be

$$\cdots \uparrow\downarrow\uparrow\downarrow\uparrow\downarrow\uparrow\downarrow\uparrow\downarrow \cdots$$

Introducing a hole will lead to

$$\cdots \uparrow\downarrow\uparrow\downarrow O \uparrow\downarrow\uparrow\downarrow \cdots$$

and after moving the hole one has (note that the kinetic term in the Hamiltonian does not flip spins)

$$\cdots \uparrow\downarrow O \uparrow\downarrow\uparrow\downarrow\uparrow\downarrow \cdots$$

Now the hole is surrounded by one up and one down spin, whereas somewhere else there are two adjacent up spins. Finally, a few exchange spin processes lead to

$$\cdots \uparrow\downarrow O \uparrow\downarrow\uparrow\downarrow\uparrow\downarrow \cdots$$

Note that the original configuration, a hole surrounded by *two* up spins has split into a hole surrounded by antiferromagnetically aligned spins (“holon”) and a domain–wall like configuration, two adjacent up spins, which contain an excess spin 1/2 with respect to the initial antiferromagnet (“spinon”). The exact solution by Lieb and Wu contains two types of quantum numbers which can be associated with the dynamics of the spinons and holons, respectively. We thus notice that spinons and holons [62, 63] have a well-defined meaning in the present one–dimensional case.

The above pictures suggest that, as far as charge motion is concerned, the Hubbard model away from half–filling can be considered as a one–dimensional harmonic solid, the motion of the holes providing for an effective elastic coupling between adjacent electrons. This picture has been shown to lead to the correct long–distance correlation functions for spinless fermions [64, 65]. For the case with spin, this suggests that one can consider the system as a harmonic solid with a spin at each site of the elastic lattice (lattice site = electron in this picture).

Let us now show that this gives indeed the correct spin correlation functions. In a continuum approximation, the spin density then becomes

$$\boldsymbol{\sigma}(x) = \sum_m \mathbf{S}_m \delta(x - x_m) , \quad (4.22)$$

where the sum is over all electrons. After a Fourier transformation of the delta function the spin–spin correlation function becomes

$$\langle \boldsymbol{\sigma}(x) \cdot \boldsymbol{\sigma}(0) \rangle = \frac{1}{(2\pi)^2} \int dq dq' \sum_{m,m'} e^{-iqx} \langle \mathbf{S}_m \cdot \mathbf{S}_{m'} e^{i(qx_m + q'x_{m'})} \rangle . \quad (4.23)$$

The exchange energy between adjacent spins is always antiferromagnetic, whether there is a hole between them or not, and consequently the low-energy spin dynamics always is that of an antiferromagnetic chain of localized spins. Under the additional assumption that the spin-spin correlations on an elastic lattice depend mainly on the average exchange constant and not so much on the fluctuations induced by motion of the electrons, the average in (4.23) factorizes into separate spin and charge factors. Following the hypothesis about harmonic motion of the electrons, we write  $x_m = R_m + u_m$ , where  $R_m = m/|1-n|$  is the average position of the  $m$ th electron and  $u_m$  the displacement with respect to this position. Note that the ‘‘harmonic solid hypothesis’’ implies that  $u_{m+1} - u_m$  is small, but not necessarily  $u_m$  and  $u_{m+1}$  separately. In the averages over atomic positions now all terms with  $q \neq q'$  vanish, and one has

$$\langle \boldsymbol{\sigma}(x) \cdot \boldsymbol{\sigma}(0) \rangle \approx \int dq \sum_{m,m'} e^{-iqx} \langle \mathbf{S}_m \cdot \mathbf{S}_{m'} \rangle e^{iq(R_m - R_{m'})} \langle e^{iq(u_m - u_{m'})} \rangle . \quad (4.24)$$

The average over  $u_m$  in (4.24) has a power law behavior:

$$\langle e^{iq(u_m - u_{m'})} \rangle \approx |m - m'|^{-\alpha(q)} ,$$

with  $\alpha(q) \propto q^2$ , i.e. it has a smooth  $q$ -dependence. On the other hand, the long-distance behavior of the spin-spin correlations of an antiferromagnetic spin chain is [66, 33, 34]

$$\langle \mathbf{S}_m \cdot \mathbf{S}_{m'} \rangle \approx (-1)^{m-m'} |m - m'|^{-1} \ln^{1/2} |m - m'| .$$

Therefore in (4.24) the  $q$ -integration is dominated by terms with  $q \approx \pi(1-n) = 2k_F$ . Replacing the weakly  $q$ -dependent exponent  $\alpha(q)$  by  $\alpha(2k_F)$  one obtains

$$\langle \boldsymbol{\sigma}(x) \cdot \boldsymbol{\sigma}(0) \rangle \approx \int dq e^{-iqx} \sum_{m,m'} \langle \mathbf{S}_m \cdot \mathbf{S}_{m'} \rangle e^{iq(R_m - R_{m'})} |m - m'|^{\alpha(2k_F)} \quad (4.25)$$

$$= \cos(2k_F x) x^{-1-\alpha(2k_F)} \ln^{1/2}(x) . \quad (4.26)$$

With the identification  $\alpha(2k_F) = K_\rho$ , this is precisely the result (2.48). We thus have shown that the spin-spin correlations of a correlated electron system can in fact be understood as those of an elastic lattice of spins. In that picture, the motion of the holes then only provides the effective elasticity for the lattice.

#### 4.3.4 The metal-insulator transition

The one-dimensional Hubbard model is insulating for  $n = 1$ ,  $U > 0$ , but conducting in all other cases. Moreover, in agreement with the discussion of section 3, the metal-insulator transition occurs in a different way according to whether the interaction strength is varied at constant carrier density or whether one varies the carrier density at constant  $U$ .

It seems worthwhile here to compare the metal-insulator transition occurring as  $n \rightarrow 1$  with other scenarios for strongly correlated fermion systems in higher

dimension (see the review by Vollhardt [67]). In the “nearly localized” picture, effective mass effects predominate and enhance both the specific heat and the spin susceptibility. Consequently, the Wilson ratio ( $1/(1 + F_0^a)$  in Fermi liquid language) remains nonzero as the metal–insulator is approached. On the other hand, in the “nearly ferromagnetic” (or paramagnon) picture, only the spin susceptibility is enhanced significantly, and therefore  $R_W$  can be much larger than unity. The behavior found here in the one–dimensional case is quite different from both these scenarios: generally  $R_W < 2$ , and approaching the metal–insulator transition  $R_W \rightarrow 0$ . This occurs because generally an enhancement of the mass of the *charge* carriers (i.e. a decrease of  $u_\rho$ ) has no influence on the spin degrees of freedom (see fig.1). This is rather straightforwardly understood in terms of *spin–charge decoupling*, as explained in the previous section: charge and spin excitations move nearly independently of each other, and in particular the spin dynamics is determined by antiferromagnetic nearest–neighbor exchange. In particular the spin susceptibility remains finite even when the mass of the charge carrier approaches infinity.

Let us discuss the metal–insulator transition in more detail. The fact that  $u_\rho$  and  $\sigma_0$  vanish linearly as  $n \rightarrow 1$  seems to be consistent with a divergent effective mass at constant carrier density because  $u_\rho \approx 1/m^*$ ,  $\sigma_0 \approx n/m^*$ . A constant carrier density is also consistent with the fact that  $k_F = \pi n/2$  is independent of  $U$ . It is *not consistent* with the hole–like sign of the thermopower as  $n \rightarrow 1$  from below, nor with the electron–like sign as  $n \rightarrow 1$  from above: if the carriers are holes, the carrier density is the density of holes:  $n^* = 1 - n$ . Treating the holes as spinless fermions, as already mentioned before, one expects  $\sigma_0 \rightarrow 0$  because  $n^* \rightarrow 0$ , and  $\gamma \rightarrow \infty$  because the density of states of a one–dimensional band diverges at the band edges. This agrees with what was found explicitly in section 4.3.1. What is not so easily understood in this picture is the fact that  $k_F$  (i.e. the location of the singularity of  $n_k$ ) is given by its free–electron value  $\pi n/2$ , rather than being proportional to  $n^*$ . One should however notice that  $n_k$  is given by the single–particle Green’s function which contains both charge and spin degrees of freedom. The location of  $k_F$  then may possibly be explained by phase shifts due to holon–spinon interaction. This is in fact suggested by the structure of the wavefunction of the exact solution [17].

The magnetic properties do not agree with what one expects from an effective mass diverging as  $n \rightarrow 1$ :  $u_\sigma$  and therefore  $\chi$  remain finite. Moreover, the NMR relaxation rate would have the behavior  $1/T_1 = \alpha T + \beta \sqrt{T}$ , where the first (Korringa) term comes from fluctuations with  $q \approx 0$ , whereas the second term comes from antiferromagnetic fluctuations with  $q \approx 2k_F$ . None of these properties is strongly influenced by the diverging effective mass observed e.g. in the specific heat. This fact is of course a manifestation of the separation between spin and charge degrees of freedom.

### 4.3.5 Other models

It is clearly interesting to go beyond the Hubbard model. A simple generalization is the “extended Hubbard model” which includes a nearest-neighbor repulsion:

$$H = -t \sum_{i,s} (a_{is}^\dagger a_{i+1,s} + a_{i+1,s}^\dagger a_{is}) + U \sum_i n_{i\uparrow} n_{i\downarrow} + V \sum_i n_i n_{i+1} \quad , \quad (4.27)$$

For this model, exact eigenvalues can not be obtained in the thermodynamic limit. The parameters in eq. (4.20) can however be calculated reliably for finite systems [68]. In particular, at quarter filling one finds a Luttinger-liquid ground state, with  $K_\rho = 1/4$  at the metal-insulator transition which occurs with increasing  $V$ , in agreement with the discussion of sec. 3.2.

Exact exponents can be obtained for the model (4.27) in the limit  $U \rightarrow \infty$ : then one has effectively spinless fermions (with  $k_F \rightarrow 2k_F$ ) with nearest neighbor interaction, a model which can be exactly solved using the Jordan-Wigner transformation into the XXZ spin chain. In particular, the  $4k_F$ -component of (2.47) is related to the correlation function of  $S_z$ . From the known results [66] one obtains, for a quarter-filled band ( $n = 1/2$ ),  $K_\rho = 1/(2 + (4/\pi) \sin^{-1}(v))$ ,  $u_\rho = \pi t \sqrt{1 - v^2} / \cos^{-1}(v)$ , with  $v = V/2|t|$ . Now  $K_\rho < 1/2$  is possible. For  $v > 1$  the system is in a dimerized insulating state. Approaching the insulating state from  $v < 1$  both  $K_\rho$  and  $u_\rho$  remain finite, i.e.  $\sigma_0$  jumps to zero at  $v = 1$ . For  $n \neq 1/2$  the parameters  $u_\rho, K_\rho$  can be obtained from numerical results [39]. Quite generally, one has  $K_\rho > 1/8$ , but  $K_\rho = 1/2$  for  $n \rightarrow 0, 1$ , independent of  $v$ . On the other hand,  $u_\rho \rightarrow 0$  as  $n \rightarrow 1/2$  for  $v > 1$ , i.e. in that case the weight of the dc conductivity goes to zero continuously, the point  $(v, n) = (1, 1/2)$  is thus highly singular. The same type of singularity also occurs at  $U = 0, n = 1$  in the Hubbard model [60]. Interestingly enough, one has  $K_\rho > 1$  if  $V < -\sqrt{2}|t|$ , i.e. a finite amount of nearest-neighbor attraction is sufficient to lead to divergent superconducting fluctuations even for infinite on-site repulsion. Also note that the singularities in  $u_\rho$  and  $K_\rho$  at  $v = -1$  (attractive interaction) represent a point of phase separation.

For the  $t - J$  model, there is one exactly solvable point ( $t = J$ ) where exact exponents can be found using the Bethe ansatz [69]. Away from this point, eq. (4.20) has been used to obtain  $K_\rho$  from numerical data [70]. It is not easy to study the metal-insulator transition occurring for  $n \rightarrow 1$  numerically, however the results are consistent with  $K_\rho = 1/2$  in this limit. For large  $J$  there is a phase with predominantly superconducting fluctuations ( $K_\rho > 1$ ).

## 5 Conclusion

In this paper, we have seen that using the bosonization method and exact solutions, one obtains a rather complete picture of many physical properties of interacting one-dimensional fermions. Probably the most important feature arising is the Luttinger liquid like behavior, characterized by non-universal power laws, together with



the separation of the charge and spin dynamics. One should also notice that there are no qualitative differences between weak and strong correlation. Metal–insulator transitions occur for commensurate bandfillings, and in particular at half–filling, for repulsive interactions. The transitions at varying particle density show qualitatively different behavior according to whether the bandfilling is an even or odd fraction.

Another type of metal–insulator transition, not discussed in detail here, occurs in the presence of disorder (see ref. [10] and references therein). In this case, as is well–known, in the absence of interactions all states are localized. Repulsive interactions enhance localization. On the other hand, sufficiently strong attraction can lead to delocalization. In cases where there is no spin gap, the transition to the delocalized conducting (in fact superconducting) state occurs at  $K_\rho > 2$ , and at the transition one has a *non–universal* value of the correlation exponent, satisfying only  $K_\rho^* \geq 2$ . In the case with spin gap, the superconducting state only occurs for  $K_\rho > 3$ . In this case, at the transition one has a *universal* value  $K_\rho^* = 3$ . One should notice that these large values of  $K_\rho$  in fact correspond to rather strong attractive electron–electron interactions, and it seems doubtful that this can be realized in an experimental system.

Unambiguous experimental observation of Luttinger liquid like behaviour and of the associated metal–insulator transitions is made difficult by the fact that all possible known candidates are in fact only *quasi*–one–dimensional, e.g. they consist of a parallel arrangement of conducting chains. At sufficiently low temperatures one thus always crosses over into a regime of effectively three–dimensional behaviour, characterized in particular by the occurrence of different kinds of ordered states. The specifically one–dimensional behaviour is thus not always easily identified. Nevertheless, a number of very interesting experiments do exist. An early and spectacular example is the observation of diffuse X–ray scattering at wavevector  $4k_F$  in the compound TTF–TCNQ [71]. In fact, in a perturbative theory, no such scattering is expected. However, within the boson picture of the Luttinger liquid, such scattering is indeed expected for strongly repulsive interaction [72, 73] (see also eq. (2.47) and the subsequent discussion). More recently, NMR data on the series of compounds  $(\text{TMTSF})_2\text{X}$  have shown Luttinger liquid like behavior [74], and in particular power–law dependence of the relaxation rate on temperature. In some of these compounds umklapp scattering is sufficiently strong to induce a (relatively small) Mott–Hubbard insulating gap, and one can then observe a crossover between high–temperature metallic and low–temperature insulating behavior at a temperature between 100K and 200K. The most recent observation concerns photoemission on  $(\text{TMTSF})_2\text{PF}_6$  [9], where the spectral density does not show a Fermi edge like behavior, but is rather reminiscent of a power–law behaviors as expected in one dimension (see eq. (2.42)). However, the observed exponent is  $\delta \approx 1$ , a value that would imply very strong electron–electron repulsion. One then would expect strong effects of umklapp scattering, i.e. typically a non–metallic conductivity. However, experiment shows good metallic behavior in the temperature region concerned. The photoemission results thus do not seem to be

fully understood. It should be pointed out here that the metal–insulator transitions observed always occur at constant band–filling, upon varying temperature, pressure, or chemical composition (which in the last two cases is equivalent to changing the interaction strength). Unfortunately, it has up to now been impossible to dope organic conductors in a sufficiently controlled way that would make the transition occurring as a function of doping observable.

Anderson has suggested that Luttinger liquid behavior might also occur in two dimensions [75], as well as in coupled chain systems [76]. Under which circumstances this suggestion is correct does not currently clear. At least for the coupled–chain case, Anderson’s suggestion is in contradiction with standard scaling [77] and renormalization group arguments [11, 78] which indicate that interchain hopping is a strongly relevant perturbation and therefore most likely will destroy the Luttinger liquid behavior.

**Acknowledgment** I’m grateful to colleagues in Orsay, in particular T. Giamarchi, D. Jérôme and J.P. Pouget, for many stimulating discussions on the subject of these notes. This work was in part supported by CEE research contract no. CII/0568.

## References

- [1] D. Jérôme and H. J. Schulz, *Adv. Phys.* **31**, 299 (1982).
- [2] A. J. Heeger, S. Kivelson, J. R. Schrieffer, and W. P. Su, *Rev. Mod. Phys.* **60**, 781 (1988).
- [3] E. H. Lieb and F. Y. Wu, *Phys. Rev. Lett.* **20**, 1445 (1968).
- [4] P. W. Anderson, *Science* **235**, 1196 (1987).
- [5] P. W. Anderson, in *Frontiers and Borderlines in Many Particle Physics*, edited by R. Broglia and J. R. Schrieffer (North Holland, Amsterdam, 1988).
- [6] J. Sólyom, *Adv. Phys.* **28**, 209 (1979).
- [7] C. Bourbonnais, *J. Phys. I France* **3**, 143 (1993).
- [8] J. P. Pouget, in *Highly Conducting Quasi-One-Dimensional Crystal Semiconductors and Semimetals*, edited by E. Conwell (Pergamon, New York, 1988), Vol. 27, p. 87.
- [9] B. Dardel *et al.*, *Europhys. Lett.* **24**, 687 (1993).
- [10] T. Giamarchi and H. J. Schulz, *Phys. Rev. B* **37**, 325 (1988).
- [11] C. Bourbonnais and L. G. Caron, *Int. J. Mod. Phys. B* **5**, 1033 (1991).

- [12] V. J. Emery, in *Highly Conducting One-Dimensional Solids*, edited by J. T. D. et al. (Plenum, New York, 1979), p. 327.
- [13] F. D. M. Haldane, *J. Phys. C* **14**, 2585 (1981).
- [14] H. A. Bethe, *Z. Phys.* **71**, 205 (1931).
- [15] M. Gaudin, *Phys. Lett. A* **24**, 55 (1967).
- [16] C. N. Yang, *Phys. Rev. Lett.* **19**, 1312 (1967).
- [17] M. Ogata and H. Shiba, *Phys. Rev. B* **41**, 2326 (1990).
- [18] H. J. Schulz, *Phys. Rev. Lett.* **64**, 2831 (1990).
- [19] H. J. Schulz, *Phys. Rev. Lett.* **71**, 1864 (1993).
- [20] J. Voit and H. J. Schulz, *Phys. Rev. B* **37**, 10068 (1988).
- [21] R. Heidenreich, R. Seiler, and D. A. Uhlenbrock, *J. Stat. Phys.* **22**, 27 (1980).
- [22] A. Luther and I. Peschel, *Phys. Rev. B* **9**, 2911 (1974).
- [23] J. Voit, *Phys. Rev. B* **47**, 6740 (1993).
- [24] V. Meden and K. Schönhammer, *Phys. Rev. B* **46**, 15753 (1992).
- [25] S. Tomonaga, *Prog. Theor. Phys.* **5**, 544 (1950).
- [26] J. M. Luttinger, *J. Math. Phys.* **4**, 1154 (1963).
- [27] D. C. Mattis and E. H. Lieb, *J. Math. Phys.* **6**, 304 (1965).
- [28] A. Luther and V. J. Emery, *Phys. Rev. Lett.* **33**, 589 (1974).
- [29] T. Giamarchi and A. J. Millis, *Phys. Rev. B* **46**, 9325 (1992).
- [30] A. M. Finkelshtein, *JETP Lett.* **25**, 73 (1977).
- [31] J. Voit, *J. Phys. C* **21**, L1141 (1988).
- [32] T. Giamarchi and H. J. Schulz, *Phys. Rev. B* **39**, 4620 (1989).
- [33] I. Affleck, D. Gepner, T. Ziman, and H. J. Schulz, *J. Phys. A* **22**, 511 (1989).
- [34] R. R. P. Singh, M. E. Fisher, and R. Shankar, *Phys. Rev. B* **39**, 2562 (1989).
- [35] V. J. Emery, A. Luther, and I. Peschel, *Phys. Rev. B* **13**, 1272 (1976).
- [36] H. J. Schulz, *Phys. Rev. B* **22**, 5274 (1980).

- [37] T. Giamarchi, Phys. Rev. B **44**, 2905 (1991).
- [38] P. M. Chaikin, R. L. Greene, S. Etemad, and E. Engler, Phys. Rev. B **13**, 1627 (1976).
- [39] F. D. M. Haldane, Phys. Rev. Lett. **45**, 1358 (1980).
- [40] J. L. Black and V. J. Emery, Phys. Rev. B **23**, 429 (1981).
- [41] M. P. M. den Nijs, Phys. Rev. B **23**, 6111 (1981).
- [42] R. Shankar, Int. J. Mod. Phys. B **4**, 2371 (1990).
- [43] D. Vollhardt, in *Correlated Electron Systems*, edited by V. J. Emery (World Scientific, Singapore, 1993), p. 57.
- [44] A. Georges and G. Kotliar, Phys. Rev. B **45**, 6479 (1992).
- [45] M. Pernici, Europhys. Lett. **12**, 75 (1990).
- [46] S. Zhang, Phys. Rev. Lett. **65**, 120 (1990).
- [47] H. J. Schulz, Phys. Rev. Lett. **65**, 2462 (1990).
- [48] F. H. L. Essler, V. E. Korepin, and K. Schoutens, Phys. Rev. Lett. **67**, 3848 (1991).
- [49] H. Shiba, Phys. Rev. B **6**, 930 (1972).
- [50] C. F. Coll, Phys. Rev. B **9**, 2150 (1974).
- [51] F. Woynarovich, J. Phys. C **16**, 5293 (1983).
- [52] F. Woynarovich, J. Phys. C **15**, 85 (1982).
- [53] C. Zhou and H. J. Schulz, to be published.
- [54] P. W. Anderson and Y. Ren, in *High Temperature Superconductivity*, edited by K. S. Bedell *et al.* (Addison Wesley, Redwood City, 1990), p. 3.
- [55] A. Parola and S. Sorella, Phys. Rev. Lett. **64**, 1831 (1990).
- [56] H. Frahm and V. E. Korepin, Phys. Rev. B **42**, 10553 (1990).
- [57] N. Kawakami and S. K. Yang, Phys. Lett. A **148**, 359 (1990).
- [58] H. Frahm and V. E. Korepin, Phys. Rev. B **43**, 5663 (1991).
- [59] D. Baeriswyl, J. Carmelo, and A. Luther, Phys. Rev. B **33**, 7247 (1986).

- [60] C. A. Stafford and A. J. Millis, Phys. Rev. B **48**, 1409 (1993).
- [61] C. A. Stafford, Phys. Rev. B **48**, 8430 (1993).
- [62] S. Kivelson, D. Rokhsar, and J. Sethna, Phys. Rev. B **35**, 8865 (1987).
- [63] Z. Zou and P. W. Anderson, Phys. Rev. B **37**, 627 (1988).
- [64] F. D. M. Haldane, Phys. Rev. Lett. **47**, 1840 (1981).
- [65] V. J. Emery, in *Correlated Electron Systems*, edited by V. J. Emery (World Scientific, Singapore, 1993), p. 166.
- [66] A. Luther and I. Peschel, Phys. Rev. B **12**, 3908 (1975).
- [67] D. Vollhardt, Rev. Mod. Phys. **56**, 99 (1984).
- [68] F. Mila and X. Zotos, Europhys. Lett. **24**, 133 (1993).
- [69] N. Kawakami and S. K. Yang, Phys. Rev. Lett. **65**, 2309 (1990).
- [70] M. Ogata, M. U. Luchini, S. Sorella, and F. Assaad, Phys. Rev. Lett. **66**, 2388 (1991).
- [71] J. P. Pouget *et al.*, Phys. Rev. Lett. **37**, 437 (1976).
- [72] V. J. Emery, Phys. Rev. Lett. **37**, 107 (1976).
- [73] P. A. Lee, T. M. Rice, and R. A. Klemm, Phys. Rev. B **15**, 2984 (1977).
- [74] P. Wzietek *et al.*, J. Phys. I France **3**, 171 (1993).
- [75] P. W. Anderson, Phys. Rev. Lett. **64**, 1839 (1990).
- [76] P. W. Anderson, Phys. Rev. Lett. **67**, 3844 (1991).
- [77] H. J. Schulz, Int. J. Mod. Phys. B **5**, 57 (1991).
- [78] M. Fabrizio, A. Parola, and E. Tosatti, Phys. Rev. B **46**, 3159 (1992).

Figure 1: Charge arrangement for a system with strong on-site and nearest-neighbor repulsion for a third-filled (top) and quarter-filled (bottom) band. Large and small dots are occupied and empty sites, respectively. Note the alternation of nearest-neighbor distances in the third-filled case.

Figure 2: “ $4k_F$ ” singlet excitation spectrum for a Hubbard chain of 40 sites with 22 and 34 electrons. The lowest “arc” from  $k/\pi = 0.05$  to  $k/\pi = 1.1$  (or  $k/\pi = 1.7$ ) is obtained by varying  $i_0$  at fixed  $I_0 = (N_0 + 1)/2$  (cf. eq. (4.13)), the higher arches correspond to increasing  $I_0$  up to  $(L - 1)/2$ .

Figure 3: “ $2k_F$ ” spin singlet ( $\triangle$ ) and triplet ( $\diamond$ ) excitation spectrum for Hubbard chains of 40 sites with 22 electrons for different interaction strengths.

Figure 4: Excitation spectra for one particle added into a Hubbard chain of 40 sites with 14, 22, and 30 electrons. The shallow arches correspond to varying  $\alpha_1$  (cf. eq. (4.15)) at constant  $I_0$ , and  $I_0$  increases from one arc to the next. Zero energy corresponds to the  $N_0 + 1$  particle ground state.

Figure 5: Excitation spectra for an added hole in a Hubbard chain of 40 sites with 22 electrons. The shallow arches correspond to varying  $\alpha_1$  (cf. eq. (4.18)) at constant  $j_1$ , and  $j_1$  increases from one arc to the next.

Figure 6: The charge and spin velocities  $u_\rho$  (full line) and  $u_\sigma$  (dashed line) for the Hubbard model, as a function of the band filling for different values of  $U/t$ : for  $u_\sigma$   $U/t = 1, 2, 4, 8, 16$  from top to bottom, for  $u_\rho$   $U/t = 16, 8, 4, 2, 1$  from top to bottom in the left part of the figure.

Figure 7: The Wilson ratio  $R_W$  for the one-dimensional Hubbard model, as a function of the band filling for different values of  $U/t$  ( $U/t = 16, 8, 4, 2, 1$  for the top to bottom curves).

Figure 8: *The correlation exponent  $K_\rho$  as a function of the bandfilling  $n$  for different values of  $U$  ( $U/t = 1, 2, 4, 8, 16$  for the top to bottom curves). Note the rapid variation near  $n = 1$  for small  $U$ .*

Figure 9: Top: *The weight of the dc peak in  $\sigma(\omega)$  as a function of bandfilling for different values of  $U/t$  ( $U/t = 1, 2, 4, 8, 16$  for the top to bottom curves).*  
 Bottom: *Variation of the relative weight of the dc peak in the total conductivity oscillator strength as a function of the bandfilling  $n$  for different values of  $U$ :  $U/t = 1$  (full line), 4 (dashed), 16 (dash-dotted), 64 (dotted), and 256 (dash-double-dotted).*

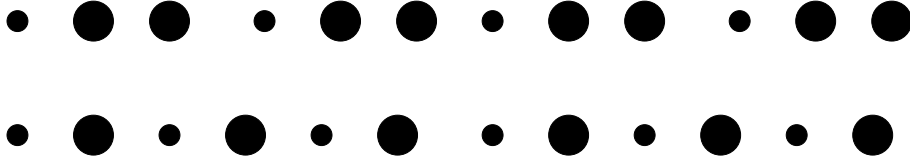


Figure 1: *Charge arrangement for a system with strong on-site and nearest-neighbor repulsion for a third-filled (top) and quarter-filled (bottom) band. Large and small dots are occupied and empty sites, respectively. Note the alternation of nearest-neighbor distances in the third-filled case.*



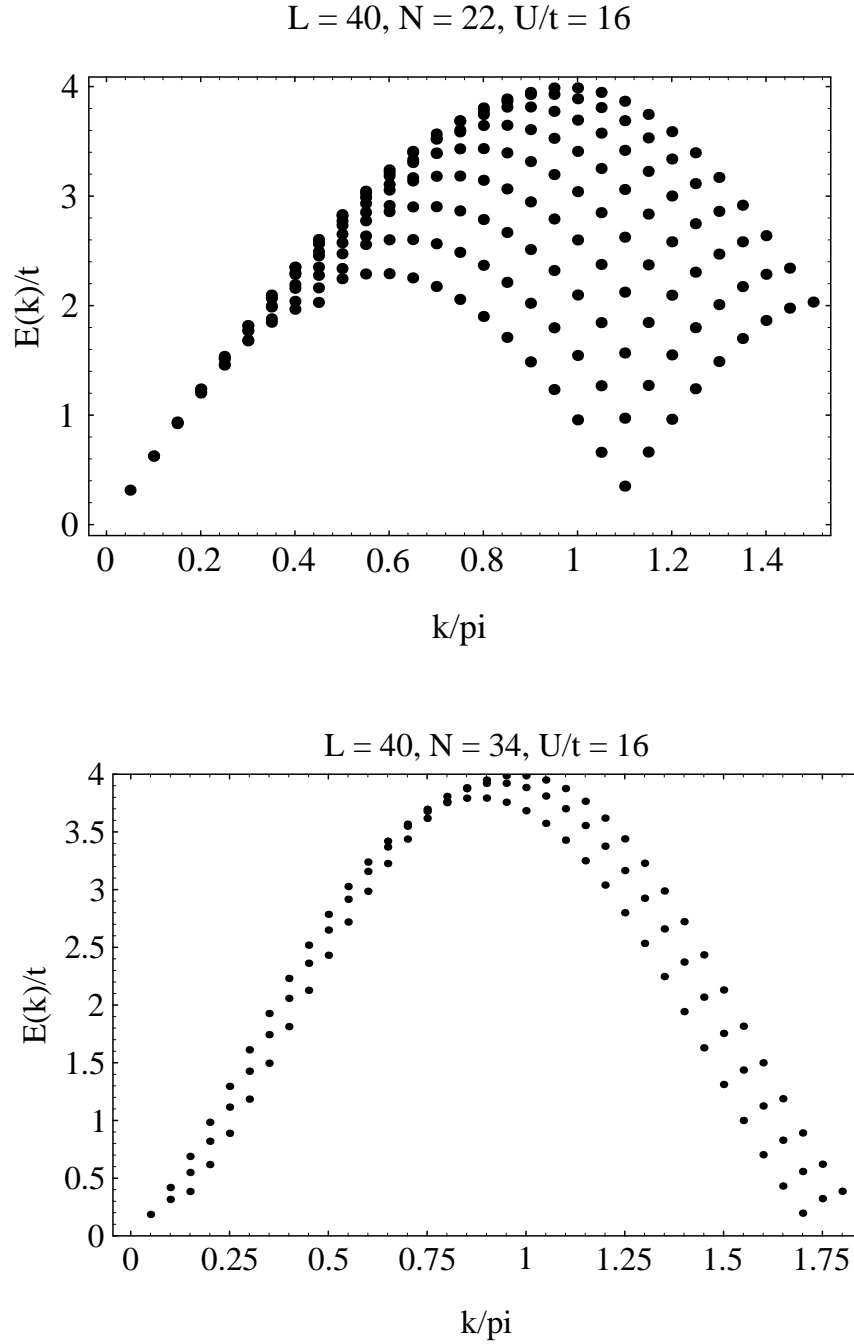


Figure 2: “ $4k_F$ ” singlet excitation spectrum for a Hubbard chain of 40 sites with 22 and 34 electrons. The lowest “arc” from  $k/\pi = 0.05$  to  $k/\pi = 1.1$  (or  $k/\pi = 1.7$ ) is obtained by varying  $i_0$  at fixed  $I_0 = (N_0 + 1)/2$  (cf. eq. (4.13)), the higher arches correspond to increasing  $I_0$  up to  $(L - 1)/2$ .

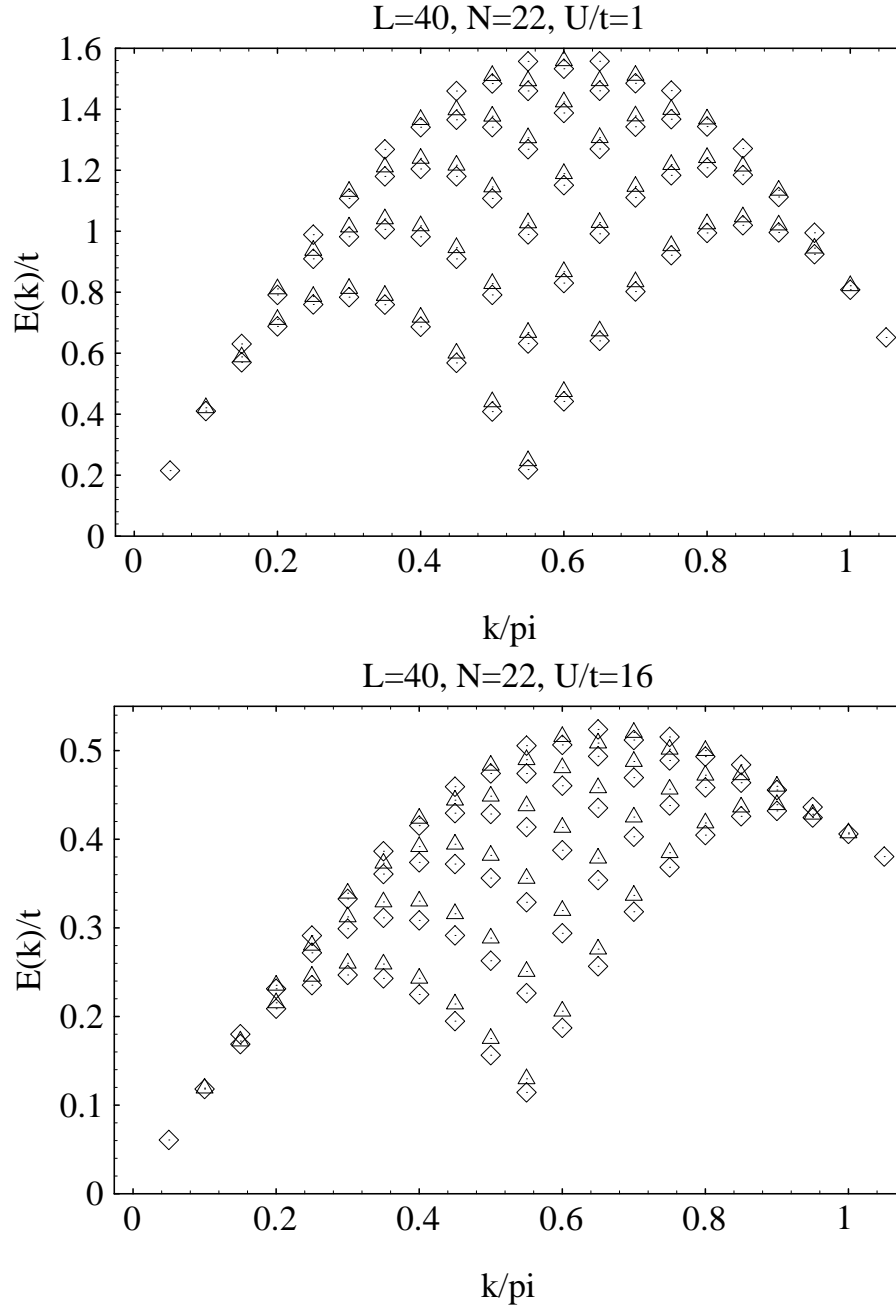


Figure 3: “ $2k_F$ ” spin singlet ( $\Delta$ ) and triplet ( $\diamond$ ) excitation spectrum for Hubbard chains of 40 sites with 22 electrons for different interaction strengths.

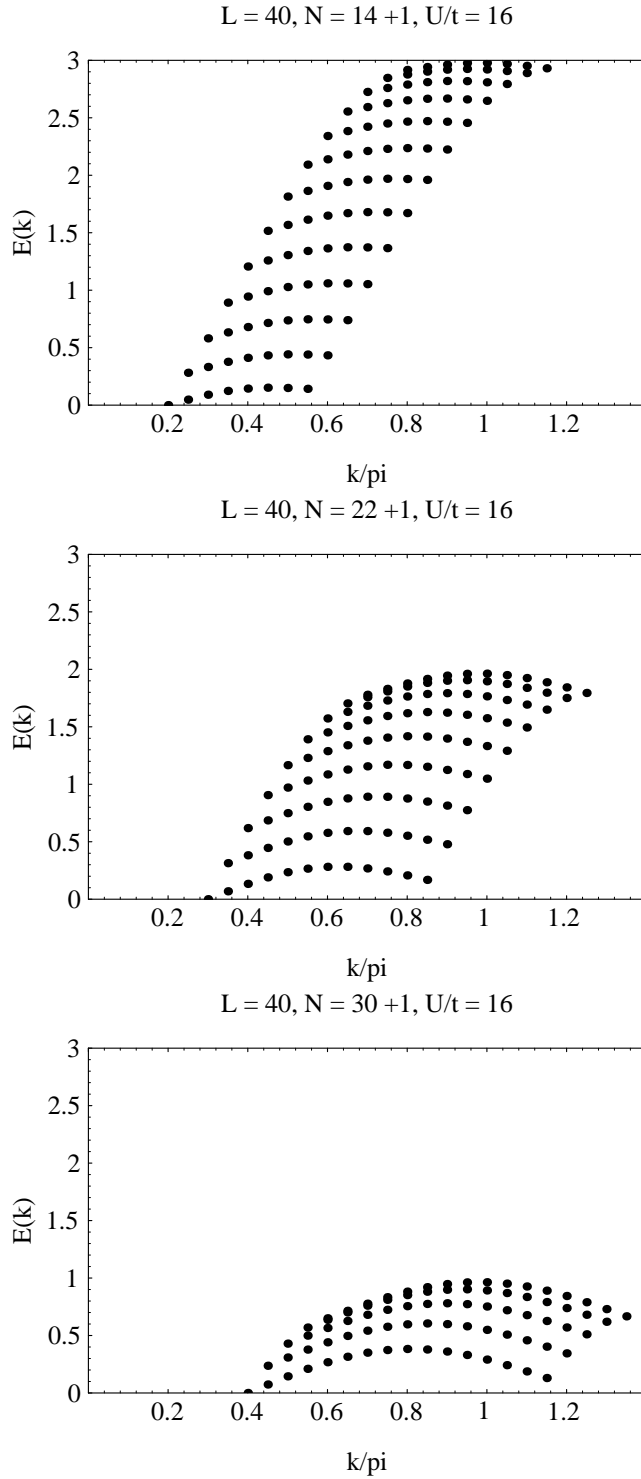


Figure 4: *Excitation spectra for one particle added into a Hubbard chain of 40 sites with 14, 22, and 30 electrons. The shallow arches correspond to varying  $\alpha_1$  (cf. eq. (4.15)) at constant  $I_0$ , and  $I_0$  increases from one arc to the next. Zero energy corresponds to the  $N_0 + 1$  particle ground state.*

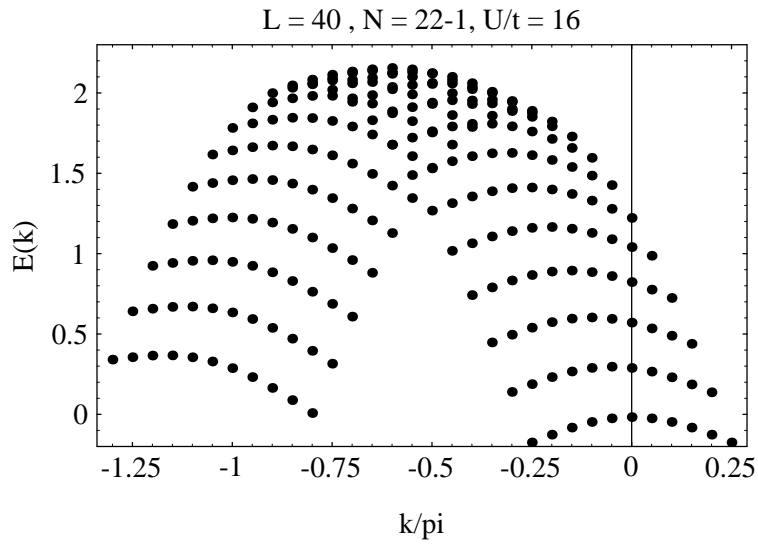


Figure 5: *Excitation spectra for an added hole in a Hubbard chain of 40 sites with 22 electrons. The shallow arches correspond to varying  $\alpha_1$  (cf. eq. (4.18) at constant  $j_1$ , and  $j_1$  increases from one arc to the next.*

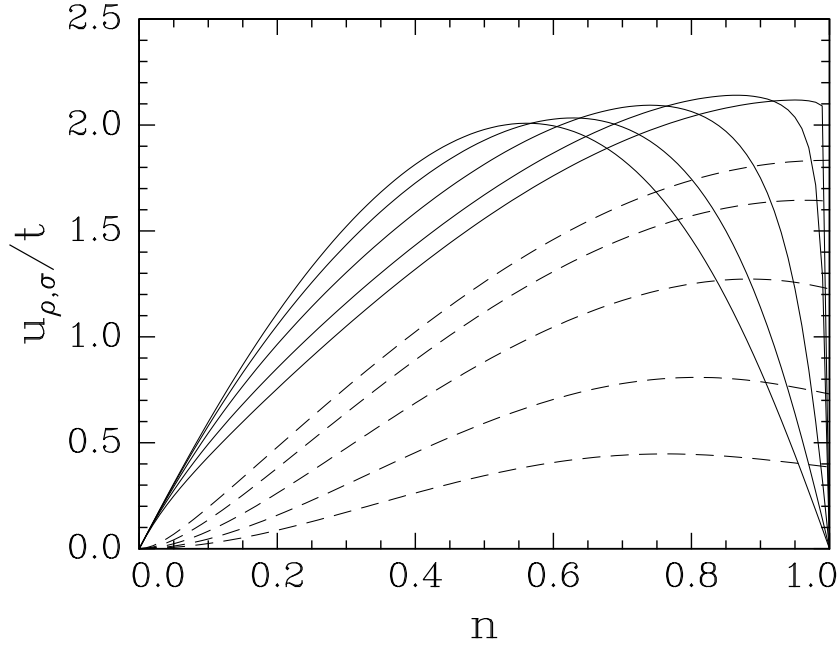


Figure 6: *The charge and spin velocities  $u_\rho$  (full line) and  $u_\sigma$  (dashed line) for the Hubbard model, as a function of the band filling for different values of  $U/t$ : for  $u_\sigma$   $U/t = 1, 2, 4, 8, 16$  from top to bottom, for  $u_\rho$   $U/t = 16, 8, 4, 2, 1$  from top to bottom in the left part of the figure.*

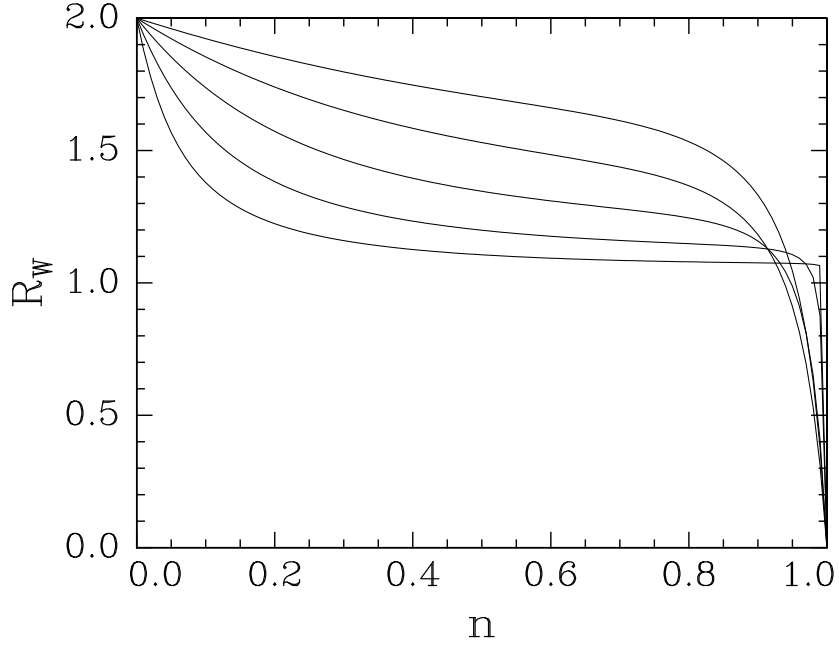


Figure 7: *The Wilson ratio  $R_W$  for the one-dimensional Hubbard model, as a function of the band filling for different values of  $U/t$  ( $U/t = 16, 8, 4, 2, 1$  for the top to bottom curves).*

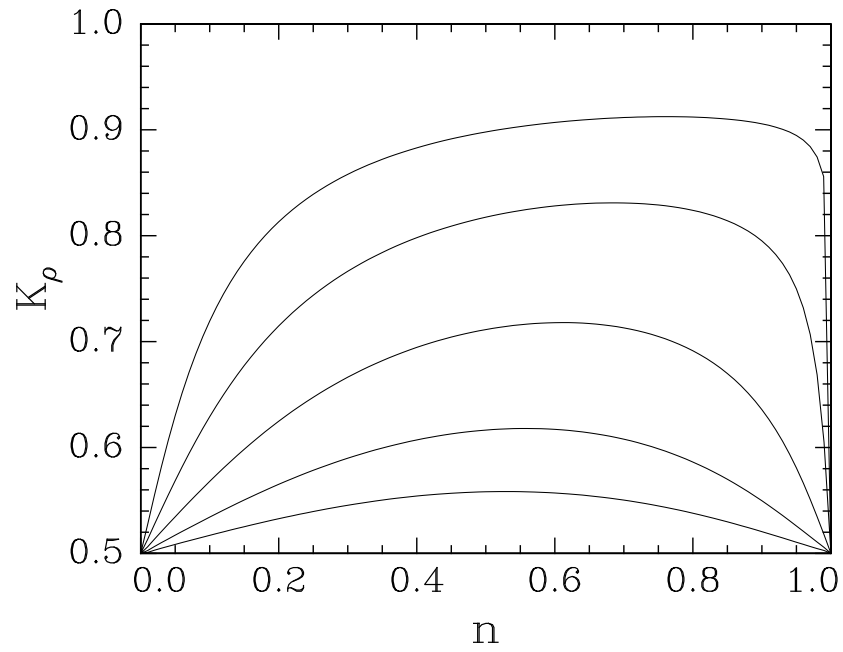


Figure 8: *The correlation exponent  $K_\rho$  as a function of the bandfilling  $n$  for different values of  $U$  ( $U/t = 1, 2, 4, 8, 16$  for the top to bottom curves). Note the rapid variation near  $n = 1$  for small  $U$ .*

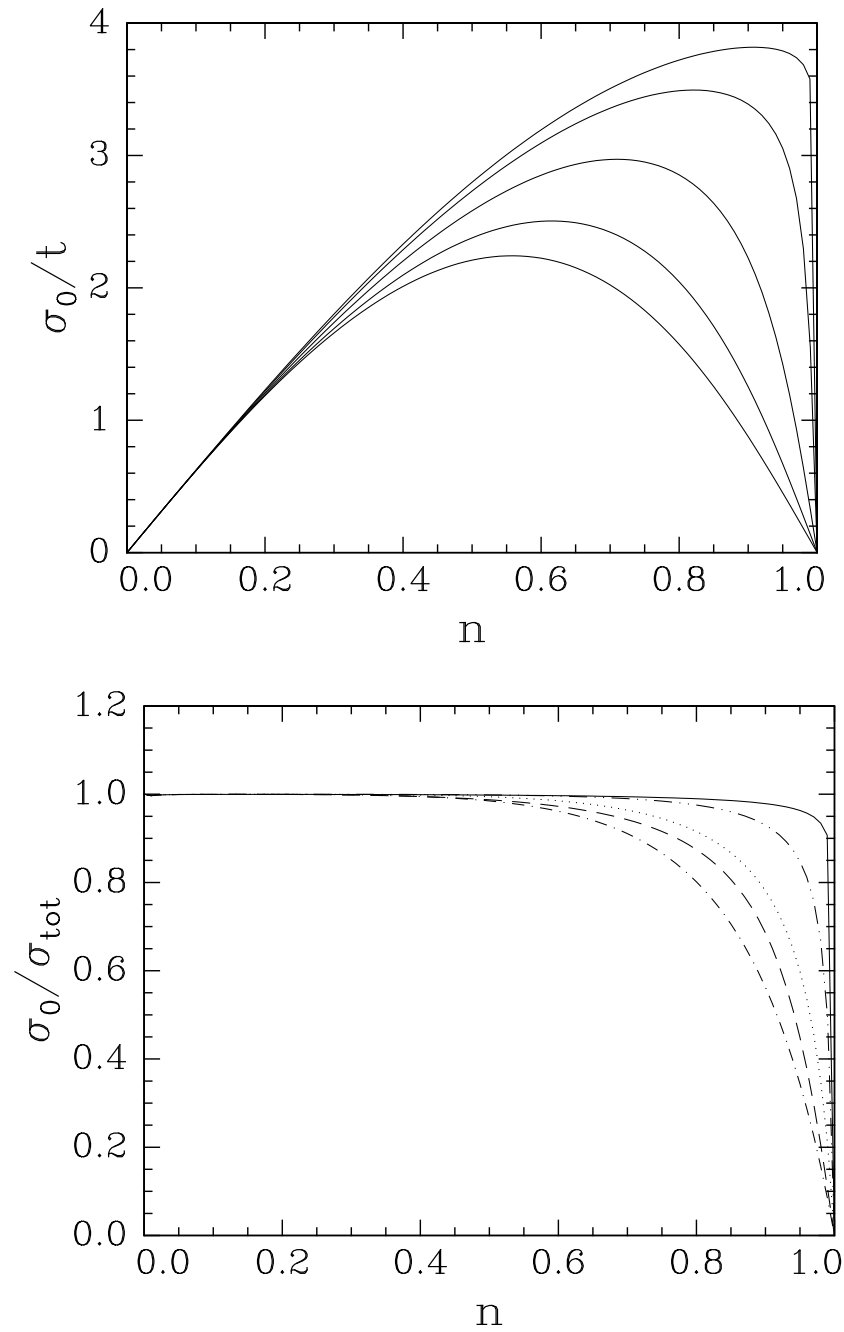


Figure 9: Top: *The weight of the dc peak in  $\sigma(\omega)$  as a function of bandfilling for different values of  $U/t$  ( $U/t = 1, 2, 4, 8, 16$  for the top to bottom curves).*

Bottom: *Variation of the relative weight of the dc peak in the total conductivity oscillator strength as a function of the bandfilling  $n$  for different values of  $U$ :  $U/t = 1$  (full line), 4 (dashed), 16 (dash-dotted), 64 (dotted), and 256 (dash-double-dotted).*